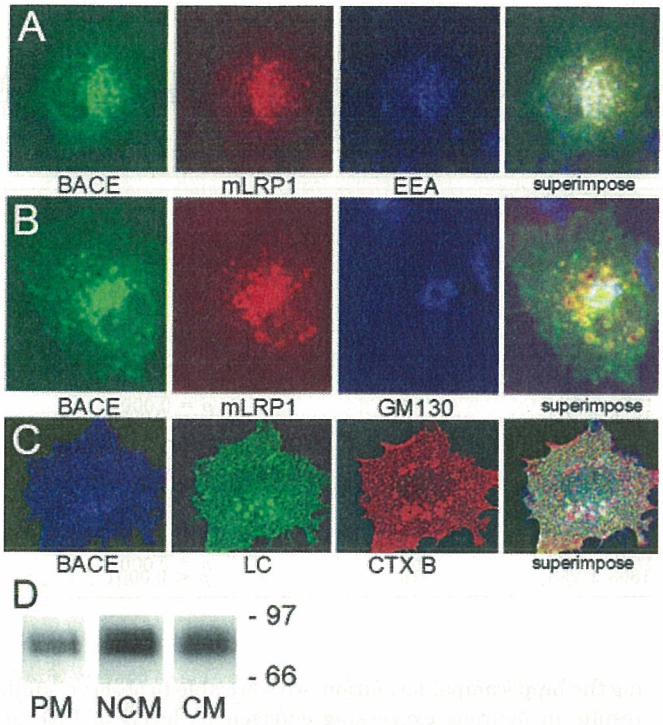

FIG. 2. **Localization of BACE and mLRP1 in transfected cells.** *A*, BACE-V5 (*green*) and mLRP1-Myc (*red*) co-transfected H4 cells were immunostained with anti-V5 mAb (visualized by Cy5) and rabbit anti-Myc Ab (visualized by Cy3) followed by a FITC-conjugated antibody to the endosomal marker EEA1 (shown in *blue*). *B*, BACE-GFP (*green*) and mLRP1-Myc (*red*) were co-transfected and then immunostained with rabbit anti-Myc (visualized by Cy3) and an antibody to the Golgi marker GM130 (visualized by Cy5, shown in *blue*). *C*, to demonstrate cell surface localization, BACE-V5 (*blue*) and Myc-(N terminus)-LC (*green*) were co-transfected and then immunostained with anti-Myc mAb (visualized by FITC) and rabbit anti-BACE-NT Ab (visualized by Cy5) without permeabilizing the cell membrane. Alexa-555-labeled cholera toxin B (*CTx-B*), used to visualize lipid rafts, was added for 20 min after thoroughly washing the primary and before adding the secondary Ab. *D*, total plasma membrane (*PM*) fraction along with CM and NCM membrane fractions immunoprecipitated with anti-LRP monoclonal 5A6 were separated on 4–12% SDS-PAGE and analyzed by immunoblot analysis using ^{125}I-anti-LRP monoclonal 11H4.

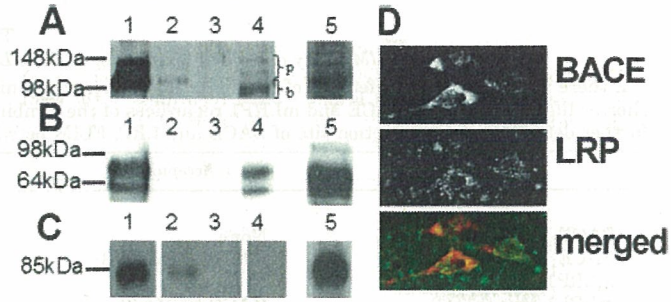

FIG. 3. **LRP and BACE in human brain.** *A*, extracts from mLRP1-Myc and BACE-V5-transfected H4 cells were immunoprecipitated with mouse anti-V5 Ab and probed with rabbit anti-Myc Ab. Anti-Myc recognizes precursor endoplasmic reticulum and Golgi forms (labeled *p*) as well as β-chains of mature proteins (labeled *b*) (positive control, *lane 5*) (29). Specific bands of all isoforms were found in pull-downs (*lane 1*) from lysates of mLRP1-Myc- and BACE-V5-expressing cells. *B*, immunoprecipitates of mLRP1-Myc were probed with an anti-BACE Ab, showing immunoreactive bands for BACE (~60 and 75kDa) in *lane 1*. The 60-kDa band represents endogenous BACE and the 75-kDa band transfected BACE-V5 (*lane 5*). *C*, human brain extracts were immunoprecipitated with rabbit anti-BACE-CT Ab and probed with 11H4. LC is recognized as an 85-kDa band brain homogenate (*lane 5*). A specific band of the same size was found after co-immunoprecipitation with anti-BACE-Ab (*lane 1*). Identical results were observed when probing with 5A6, another LC-specific Ab (data not shown). Negative controls as described above are shown in *lanes 2* and *3*. Supernatants are shown in *lane 4*. *D*, BACE and LRP co-localization in human brain tissue is shown by confocal microscopy.

blocked in 5% nonfat dried milk. mLRP1-Myc was detected by rabbit anti-Myc Ab. BACE was detected by rabbit anti-BACE-NT Ab. Secondary antibodies conjugated to horseradish peroxidase were applied and visualized by chemiluminescence. The Massachusetts Alzheimer Disease Research Center Brain Bank provided temporal cortex. Our protein solubilization procedure was adapted from previously reported studies (35) with minor modifications. The tissue was homogenized at 1 ml/100 mg tissue in ice-cold TEVP-sucrose buffer (containing 10 mM Tris, pH 7.4, 5 mM NaF, 1 mM Na_3VO_4, 1 mM EDTA, 1 mM EGTA, and 320 mM sucrose). The homogenates were centrifuged at 4 °C, and the supernatants were removed. The pellets were resuspended in 800 μl of TEVP with 1% SDS, sonicated for 10 s, and then boiled for 5 min. The samples were centrifuged, and the supernatant was collected for immunoprecipitation after the protein concentration was determined by protein assay (Bio-Rad). Co-immunoprecipitation in human brain tissue was performed as described above with rabbit anti-BACE-CT as pull-down Ab and probed with 11H4 mAb.

FRET Measurements using Fluorescence Lifetime Imaging Microscopy (FLIM)—FRET is observed when two fluorophores are in very close proximity, *i.e.* <0 nm. FRET measurements using FLIM relies on the observation that fluorescence lifetimes (the time of fluorophore emission after brief excitation, measured in picoseconds) are shorter in the presence of a FRET acceptor. We have utilized a new FLIM technique that can detect protein-protein proximity using multiphoton microscopy (36, 37). A mode-locked Ti-sapphire laser (Spectra Physics) sends a ~100-fs pulse every ~12.5 ns to excite the fluorophore. Images were acquired using a Bio-Rad Radiance 2000 multiphoton microscope. We used a high speed Hamamatsu MCP detector (MCP5900; Hamamatsu, Ichinocho, Japan) and hardware/software from Becker and Hickl (SPC 830, Berlin, Germany) to measure fluorescence lifetimes on a pixel-by-pixel basis. Excitation at 800 nm was empirically determined to excite GFP, Alexa 488 and FITC, but not Cy3. Donor fluorophore (GFP, Alexa 488, or FITC) lifetimes were fit to two exponential decay curves to calculate the fraction of fluorophores within each pixel that interact with an acceptor. As a negative control, GFP, Alexa 488, or FITC lifetimes were measured in the absence of acceptor (Cy3), which showed lifetimes equivalent to GFP, Alexa 488-IgG, or FITC IgG alone, in solution or with co-transfection with an empty vector (pEGFP) measured in the presence of Cy3-labeled BACE-V5 or LC-Myc. No bleedthrough or mis-excitation of Cy3 was observed under these conditions. Statistical testing was performed by Student's *t* test.

Internalization Assay—To quantitate BACE internalization we modified a previously reported protocol (38). CHO 13-5-1 (LRP-null cells) were grown to 70% confluency in 6-well plates and transiently transfected with Myc-BACE and either empty vector or LC-GFP. Cells were then washed once with ice-cold PBS containing 1 mM $CaCl_2$ and 1 mM $MgCl_2$, 0.2% bovine serum albumin, and 5 mM glucose (PBS++++) and 0.4 μg/ml biotinylated Myc-mAb (Upstate Biotechnologies) in PBS++++ was applied for 30 min on ice. After that the cells were allowed to endocytose at 37 °C for the indicated times. Returning the plates to ice stopped endocytosis. Surface biotin was masked with streptavidin (Roche Applied Science) for 1 h on ice. Avidin was quenched with 0.5 mg/ml biocytin (Sigma). Cells were harvested in blocking buffer (1% Triton X-100, 0.1% SDS, 0.2% bovine serum albumin, 50 mM NaCl, 1 mM Tris, pH 7.4) and incubated on IgG-coated 96-well plates at 4 °C overnight. After three washes in PBS, the plates were incubated in streptavidin-peroxidase 1:5000 (Roche Applied Science) in blocking buffer for 1 h. After another wash cycle 3× in PBS, the plates were incubated with 200 μl of 10 mg of *o*-phenyldiamine HCl (Sigma), 10 μl of 30% H_2O_2 (Sigma) in 25 ml of 50 mM Na_2HPO_4, 27 mM citrate, pH 5.0. The reaction was terminated by the addition of 50 μl of H_2SO_4 and the A_{490} was read. BACE internalization was then graphed as the percentage of internalized Myc-BACE of total surface Myc-BACE.

LRP Ectodomain Secretion Assay—HEK cells passaged into 12-well plates were transfected with a β-galactosidase reporter, LRPβ-fused N-terminally to secreted alkaline phosphatase and either empty vector, BACE, or a catalytically inactive BACE mutant. Each condition was transfected in triplicate except for siRNA experiments, which were transfected in duplicate. Media was changed 24 h later, and then collected after another 24 h. Measurement of SEAP activity in the conditioned media was carried out in triplicate by chemiluminescent assay (Roche Applied Science) according to the manufacturer's instructions. SEAP activity was normalized to β- galactosidase activity, which

TABLE I

FLIM assay data for proximity of various LRP and BACE-constructs in transfected H4 cells

If there is no interaction, lifetimes of the donor fluorophore are similar to the negative control (lacking the acceptor fluorophore). Statistically shorter lifetimes between BACE and mLRP1 regardless of the combination of fluorophore at their C terminus indicate FRET between them. To further determine the interaction site of BACE and LRP, FLIM between deletion constructs was performed.

Donor	Acceptor	Lifetime	*n*	Significance (compared to control)
		ps mean ± S.D.		
BACE-V5 (FITC)	None	2334 ± 72	12	—[a]
BACE-V5 (FITC)	mLRP1-Myc (Cy3)	2153 ± 55	11	$p < 0.0001$
mLRP1-Myc (FITC)	None	2260 ± 109	17	—[a]
mLRP1-Myc (FITC)	BACE-V5 (Cy3)	1703 ± 401	15	$p < 0.0001$
mLRP1-GFP	None	2164 ± 10	5	—
mLRP1-GFP	BACE-V5 (Cy3)	1165 ± 8	5	$p < 0.0001$
mLRP1-GFP	Myc-BACE (Cy3)	2247 ± 102	5	NS[b]
BACE-GFP	None	2284 ± 20	6	—
BACE-GFP	mLRP1-Myc (Cy3)	1756 ± 50	4	$p = 0.0004$
pEGFP-N1-vector	None	2157 ± 71	5	—
pEGFP-N1-vector	BACE-V5 (Cy3)	2106 ± 37	5	NS
pEGFP-N1-vector	mLRP1-Myc (Cy3)	2138 ± 101	5	NS
Myc-LC (11H4-FITC)	None	2305 ± 69	15	—
Myc-LC (11H4-FITC)	BACE-V5 (Cy3)	2100 ± 148	15	$p < 0.0001$
LRP165-Myc (11H4-FITC)	None	2316 ± 86	13	—
LRP165-Myc (11H4-FITC)	BACE-V5 (Cy3)	1803 ± 283	16	$p < 0.0001$

[a] —, signifies control condition.
[b] Not significant.

was measured by hydrolysis of *o*-nitrophenyl-β-D-galactopyranoside in cells lysed with reporter lysis buffer (Promega). Pharmacologic inhibition of LRP cleavage was assessed after overnight treatment with vehicle (Me_2SO) or a cell-permeable, peptidomimetic inhibitor of BACE (Calbiochem) (39).

Western Blotting—N2a cells co-transfected with LC-Myc and either empty vector, BACE, or a catalytically inactive BACE mutant and treated with 1 μM γ-secretase inhibitor DAPT (40) for 12 h (a generous gift from M. Wolfe, Brigham and Women's Hospital, Boston, MA) were lysed in 1% Triton X-100 in TBS buffer and proteinase inhibitor tablets (Roche Applied Science) and then loaded onto 4–20% Tris-glycine polyacrylamide gels (Novex) under denaturing and reducing conditions. The proteins were transferred to polyvinylidene difluoride membrane and LRP light chain was detected by rabbit anti-Myc Ab with Alexa 680 (Molecular Probes) goat anti-rabbit secondary and visualized on a Licor Odyssey near-infrared gel reader (Lincoln, Nebraska).

Luciferase Assay—HEK293 cells were transfected with LRP-Gal4-VP16 (LRP-GV) in the absence or presence of BACE and relative luciferase activity determined (28). Activity relative to β-galactosidase is shown and averaged for triplicate transfection. In all cases transfection was confirmed by immunoblotting.

RESULTS

Localization of BACE and LRP Constructs—We first tested the localization of BACE and LRP in co-expressing H4 cells. When expressed individually, both mLRP1 and BACE were localized mainly in punctate structures in the cells. mLRP1-positive structures largely overlapped with BACE-positive structures when they were co-expressed. To determine the subcellular distribution we immunostained co-expressing H4 cells with organelle markers or, in cell surface stained without Triton X-100 treatment, Alexa555-labeled CTx-B as a raft marker. mLRP1 and BACE co-localized in the endosomal compartments stained by EEA1 (Fig. 2*A*). To a lesser extent, the Golgi marker GM130 also overlapped with mLRP1 and BACE (Fig. 2*B*). On the cell surface Myc-LC and BACE are partly co-localized with one another in lipid rafts. The results of the immunocytochemistry suggest that LC and BACE are co-localized in distinct compartments of the cell including lipid rafts (Fig. 2*C*), Golgi and prominently in the endosomal compartment.

To confirm that LRP localizes to lipid rafts we prepared total membrane and separated CM and NCM fractions using an optiprep gradient. LRP was present in caveolae as well as in noncaveolae fractions (Fig. 2*D*), which is in accordance with our confocal data showing partial overlap with the lipid raft marker CTx-B. We then looked for co-localization under physiological conditions. By staining human brain sections, including the hippocampal formation, we were able to observe similar results in neurons expressing endogenous levels of LRP and BACE (Fig. 3*D*).

Co-immunoprecipitation of BACE and LRP in Human Brain Tissue—From the immunohistochemical experiments that showed robust co-localization in both transfected cells and human brain tissue (Fig. 3*D*), we hypothesized that there may be a close interaction between LRP and BACE. To test whether LRP interacts with BACE, we immunoprecipitated BACE from co-transfected H4 cells and probed for mLRP1 (*lane 1*), controlling for nonspecific interactions by assessing lysates incubated without the pull-down antibody (*lane 2*) or pure lysis buffer (*lane 4*). Immunoreactive bands of ~100 kDa (resembling mature furin-cleaved mLRP1-Myc) and ~140 kDa (resembling unprocessed Golgi and ER forms of mLRP1-Myc) (29) were detected in the immunoprecipitated sample and the whole cell lysate (Fig. 3*A*, *lane 4*). To confirm this interaction, the complementary pull-down experiment was performed. mLRP1 immunoprecipitates were probed by an anti-BACE Ab with the same controls. The doublet bands of ~60 and 75 kDa were detected only in *lane 1* and in the control lysate lane (Fig. 3*B*), suggesting that BACE is present in the mLRP1 immunoprecipitates. The 60-kDa band represents endogenous BACE, whereas the 75-kDa band represents transfected BACE containing a V5-His tag.

To demonstrate a direct interaction of LRP and BACE under physiological conditions in brain, where BACE function is presumed to be important in the pathogenesis of Alzheimer disease, we immunoprecipitated BACE from human brain tissue and probed with an antibody to the LRP light chain. A strong immunoreactive band of ~85 kDa (the expected size of the mature endogenous light chain of LRP, *i.e.* furin-cleaved form) (29) was detected in the sample lane (Fig. 3*C*, *lane 1*). Control precipitate from samples lacking anti-BACE Ab (*lane 2*) showed only a weak immunoreactive band, and samples lacking cell extract (*lane 3*) did not contain this band. Thus, endogenous LRP and BACE co-immunoprecipitate.

Interaction of LRP and BACE by FLIM Analysis—We next used an alternative technique to probe protein-protein proximity to test the idea that the LRP-BACE interaction detected by co-immunoprecipitation occurs in specific cell compartments, and to further evaluate the biochemical parameters of this interaction. We utilized FLIM, a morphology-based FRET tech-

nique that can reveal close protein-protein proximity in intact cells. Fluorescence lifetime is influenced by the surrounding microenvironment and is shortened in the immediate vicinity of a FRET acceptor molecule. The degree of lifetime shortening can be displayed with very high spatial resolution in a pseudocolor-coded image. As shown in Fig. 2, double immunostaining showed subcellular compartment co-localization of BACE and LRP predominantly in endosomal compartments, but this does not necessarily imply a close interaction. We measured changes in the lifetime of the donor fluorophore (either FITC, Alexa 488, or GFP) under different experimental conditions. In the absence of an acceptor fluorophore, the lifetime of FITC conjugated to IgG (hereafter referred to simply as FITC) is ~2300 ps, GFP ~2200 ps, and Alexa 488 is ~1900 ps. If an acceptor fluorophore is present but remains too distant from the donor (*i.e.* there is no interaction), donor lifetimes remain in this range. The lifetime of FITC attached to the C terminus of BACE-V5 alone (2334 ± 72 ps) was significantly shortened when co-expressed mLRP1-Myc was C-terminally labeled by Cy3 (2153 ± 55 ps, $p < 0.0001$), indicating FRET between the two fluorophores (Table I). Equivalent results were obtained when BACE was tagged with GFP and when the acceptor and donor fluorophores were exchanged (Table I). In order to test the idea that the decrease in lifetime observed in the mLRP1-GFP/BACE-V5 FLIM assay was because of FRET, we performed an additional control. mLRP1-GFP and Myc-BACE co-transfected cells were stained with anti-Myc Ab, then labeled with Cy3. In this experiment, the Myc tag was at the N terminus of BACE, across the membrane and, therefore, too distant from the C-terminal GFP on mLRP1-GFP to be detected by FRET. Although there was striking co-localization, no lifetime change was observed. This experiment demonstrates the specificity of the proximity assay in this FLIM-based method of measuring FRET.

FLIM allows analysis of FRET localization by recording the distribution of donor lifetimes on a pixel-by-pixel basis. FITC bound to BACE-V5 in the absence of acceptor has a uniform lifetime and a single lifetime peak (Fig. 4*A*); in the presence of mLRP1-Cy3 acceptor, FITC has two distinct lifetimes and is faster, representing "FRETting" molecules (Fig. 4*B*). Examination of the FLIM images of transfected cells suggests that LRP and BACE interact (red pseudocolor) at the cell surface and in endosomal compartments. Because LRP and BACE co-localize in lipid rafts at the cell surface, we suggest that the interaction detected by FLIM also is lipid raft-associated.

Indeed, additional experiments in which only cell surface Myc-LC (N-terminal Myc) and BACE-NT are immunostained demonstrate FRET (Table II) between BACE and LRP specifically in punctuate structures at the cell surface (Fig. 5*B*). To test the hypothesis that this interaction occurs in rafts we cholesterol depleted the cells and repeated the cell surface FLIM experiment. Cholesterol depletion weakened the interaction of BACE and LRP at the cell surface (Fig. 5*C*). This result strongly suggests that BACE and LRP interact on the cell surface distinctively in lipid rafts.

To further confirm the physiologic interaction of LRP and BACE we performed FLIM in untransfected N2a cells as well as primary cortical neurons, which have relatively abundant BACE and LRP; Alexa 488 was chosen as donor fluorophore because it is somewhat brighter than FITC under the conditions utilized. Statistically shorter lifetimes of the donor in N2a cells (Alexa 488) attached to the C terminus of BACE in the presence of C-terminally Cy3-labeled LRP (1492 ± 293 ps, $p < 0.0001$) compared with only Alexa 488-labeled BACE (1868 ± 116 ps) as well as in FITC-labeled primary neurons attached to the C terminus of BACE in the presence of C-terminally Cy3-labeled LRP (2055 ± 103 ps, $p \leq 0.005$) compared with only FITC-labeled BACE (2193 ± 105 ps) indicate FRET between endogenously expressed proteins (Table III). In the absence of acceptor, Alexa 488 has a uniform lifetime; in the presence of acceptor a second peak appears, reflecting an interaction (Fig. 4, *C–F*). The interaction, pseudocolored red, also appears to be stronger in the distal compartments at or near the cell surface. This result demonstrates close protein-protein interaction between endogenous LRP and endogenous BACE at the cell surface in a neuronal cell type, paralleling the co-immunoprecipitation results.

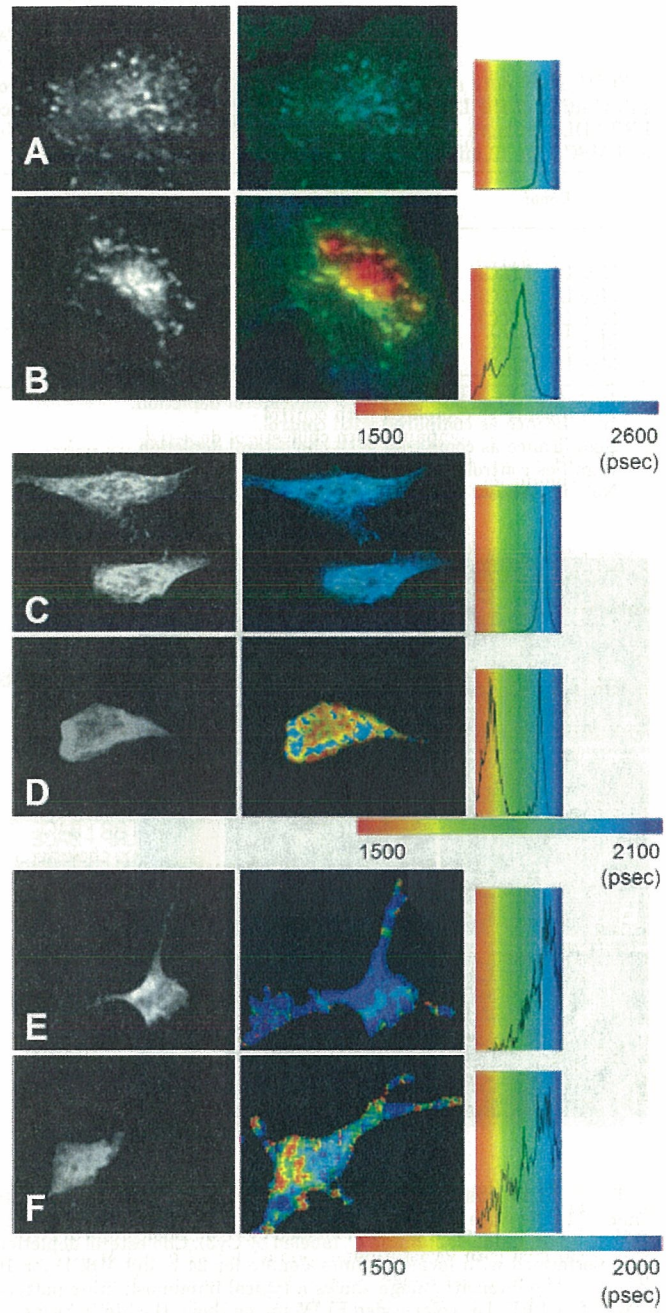

FIG. 4. **FLIM analysis of the proximity between LRP and BACE within cells.** H4 cells were co-transfected with mLRP1-Myc (*A*, unlabeled; *B*, labeled by Cy3) and BACE-V5 (labeled by FITC). N2a cells were stained for endogenous LRP with 11H4 (labeled by Cy3) and anti-BACE CT Ab (labeled by Alexa 488) for the analysis (*D*) or only with the donor fluorophore in the negative control (*C*). Primary neurons were stained for endogenous LRP with 11H4 (Cy3) and Anti-BACE CT Ab (FITC) for the analysis (*F*) or only with the donor fluorophore (*E*). The intensity of the images shows the standard immunostaining pattern for BACE. The color-coded FLIM image shows the lifetimes (ps) of FITC in the presence or absence of donor Cy3.

TABLE II
FLIM assay data

FLIM assay data showing the proximity of LC and BACE and strong weakening of this proximity by cholesterol depletion (Chol. depl.) and substitution of the LRP intracellular domain by LDLR in cell surface staining. H4 cells were co-transfected with Myc-(N terminus)-LC or an LRP-LDLR chimera (labeled by FITC) and BACE-V5 (labeled by Cy3). Cholesterol depletion was performed with lovastatin/mevalonate for 24 h and MβCD for 10 min.

Donor	Acceptor	Chol. depl.[a]	Lifetime	*n*	Significance	
			ps mean ± S.D.			
Myc-LC (FITC)	None	−	2317 ± 109	21	—[d]	—[d]
Myc-LC (FITC)	BACE-NT (Cy3)	−	2023 ± 173	23	$p < 0.0001$[b]	$p < 0.0001$[c]
Myc-LC (FITC)	BACE-NT (Cy3)	+	2203 ± 83	21	$p < 0.001$[b]	—[d]
Myc-LC-LDLR	None	−	2335 ± 111	8	—[d]	$p < 0.005$[c]
Myc-LC-LDLR	BACE-NT (Cy3)	−	2243 ± 143	8	NS[e]	—[d]

[a] Presence (+) or absence (−) of cholesterol depletion.
[b] Significance as compared with control.
[c] Significance as compared with cholesterol depletion.
[d] Signifies control condition.
[e] Not significant.

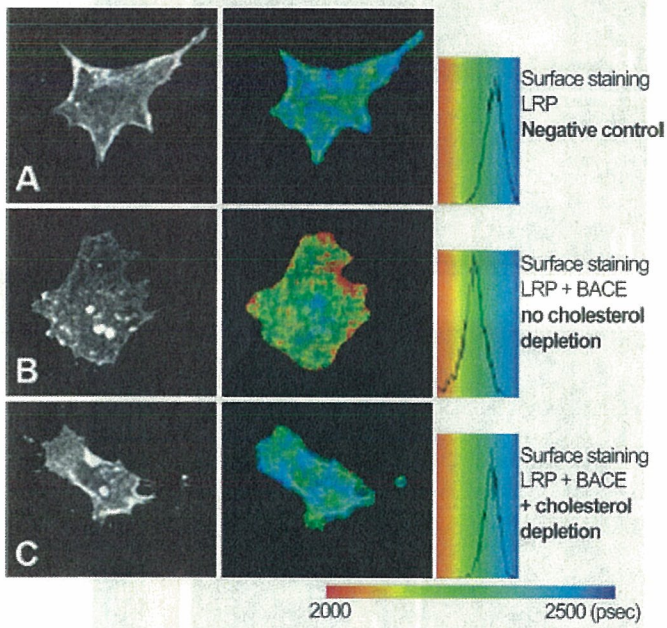

FIG. 5. **FLIM analysis of LC and BACE proximity on cell surface.** H4 cells were co-transfected with Myc-LC (labeled by FITC) and BACE-V5 (*A*, unlabeled; *B* and *C*, labeled by Cy3). Cholesterol depletion was performed with lovastatin/mevalonate for 24 h and MβCD for 10 min (*C*). The intensity image shows a typical immunostaining pattern for surface LRP. The color-coded FLIM image shows the lifetimes (ps) of FITC in the absence (*A*) or presence of the acceptor Cy3 (*B* and *C*). The shorter FITC lifetimes, represented by red-yellow pseudocolor, appear in distinct spots on the cell surface (*B*), and can be abolished by cholesterol depletion (*C*).

To identify the domain of LRP interacting with BACE, we utilized LRP deletion constructs. LC, which contains the β-chain of LRP, and LRP165, a construct that contains only the 100 amino acid intracellular domain, the transmembrane domain and a very small extension beyond the membrane, both interacted strongly with BACE (Table I). This result implicates the intracellular or the transmembrane domain of LRP as the site of interaction. To further test this hypothesis, we utilized a chimeric protein in which the extracellular and transmembrane domains of LC are fused to the intracellular domain of the low density lipoprotein receptor (LDLR) (Fig. 1) and performed FLIM on the cell surface as described above. This construct did not FRET with BACE (Table II), further supporting the importance of the intracellular domain of LRP for this interaction.

There are several scaffold/adaptor proteins known to interact with LRP including Fe65 (22, 23, 41) and mammalian disabled 1 (mDab1) (23). If the intracellular domain is responsible for the interaction between LRP and BACE, these adaptor proteins may play a role in the interaction. We have demonstrated previously that LRP and Fe65 interact using a FRET based cell assay (22), and that Fe65 is responsible for mediating an LRP-Fe65-APP heterotrimeric complex. We therefore examined the possibility that these molecules may interact with BACE by the FRET assay. However, under the conditions utilized we did not detect any FRET between BACE and Fe65 or between BACE and mDab1 (data not shown). Recent data also suggest that phosphorylation of BACE at Ser^{498} changes its trafficking possibly by altering its interactions with GGA by its C-terminal dileucine motif (30, 42). We generated the S498D, S498A, and L499A/L500A mutants of BACE to evaluate if these mutants, which mimic or block phosphorylation of Ser^{498} (15), alter interaction with LRP. No changes in FRET measures were observed with these manipulations (data not shown).

BACE Internalization Assay—Because we observed LRP-BACE interactions dependent on a domain of LRP that mediates APP endocytosis, we hypothesized that LRP might also influence BACE endocytosis and thereby regulate APP cleavage. In order to assess the effect of LRP on BACE endocytosis we assessed internalization of BACE after biotinylation of its N-terminal Myc tag at the cell surface and assayed internalized *versus* cell surface BACE over time (Fig. 6). Co-transfection with LC did not enhance BACE internalization from the cell surface in LRP-null CHO cells (13–5-1) in contrast to known enhancement of APP endocytosis with LC (20). The same results were obtained using PEA13 (LRP−/−) fibroblasts (data not shown). Thus it appears that BACE internalization is not mediated by LRP under these conditions.

LRP Shedding—Because LRP is a known γ-substrate, we hypothesized that it might also be cleaved by β-secretase. In order to assess the effect of BACE and LRP interaction on LRP processing, we measured shedding of the extracellular domain of LRP with the cDNA of SEAP fused to the N terminus of the LRP β-chain. An analogous construct has been used to study BACE cleavage of APP (43). After co-transfection of the SEAP-LRP construct with a β-galactosidase reporter construct and either empty vector, WT-BACE or BACE D93/289A, SEAP activity was measured in the medium and normalized to β-galactosidase activity. WT-BACE led to a significant increase in LRP ectodomain shedding compared with baseline, whereas, as expected, catalytically inactive BACE D93/289A exhibited no effect (Fig. 7*A*). To confirm that LRP is cleaved by BACE, we used two additional approaches. Overnight treatment with a cell-permeable BACE inhibitor (39) reduced LRP cleavage

TABLE III
FLIM assay data showing the proximity of endogenous LRP and BACE in N2a cells and in primary neurons.

	Donor	Acceptor	Lifetime	*n*	Significance (compared to control)
			ps mean ± S.D.		
N2a cells	BACE-CT (Alexa 488)	None	1868 ± 116	20	—[a]
	BACE-CT (Alexa 488)	11H4 (Cy3)	1492 ± 293	20	$p < 0.0001$
Primary neurons	BACE-CT (FITC)	None	2193 ± 105	15	—[a]
	BACE-CT (FITC)	11H4 (Cy3)	2055 ± 108	10	$p \leq 0.005$

[a] — Signifies control condition.

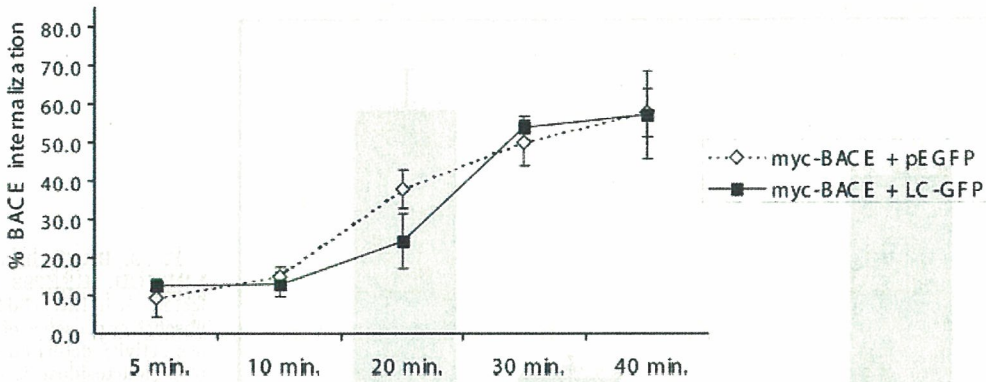

FIG. 6. **BACE internalization assay.** Internalization of biotinylated Myc-BACE was monitored over 40 min in LRP-null CHO (13-5-1) cells co-transfected with either empty vector (pEGFP ◇) or LC-GFP (◆). No change of the basic endocytosis rate of BACE with LRP co-transfection was observed. Given are the means and S.D. of one of three independent assays. Both transfection and measurement were carried out in triplicate.

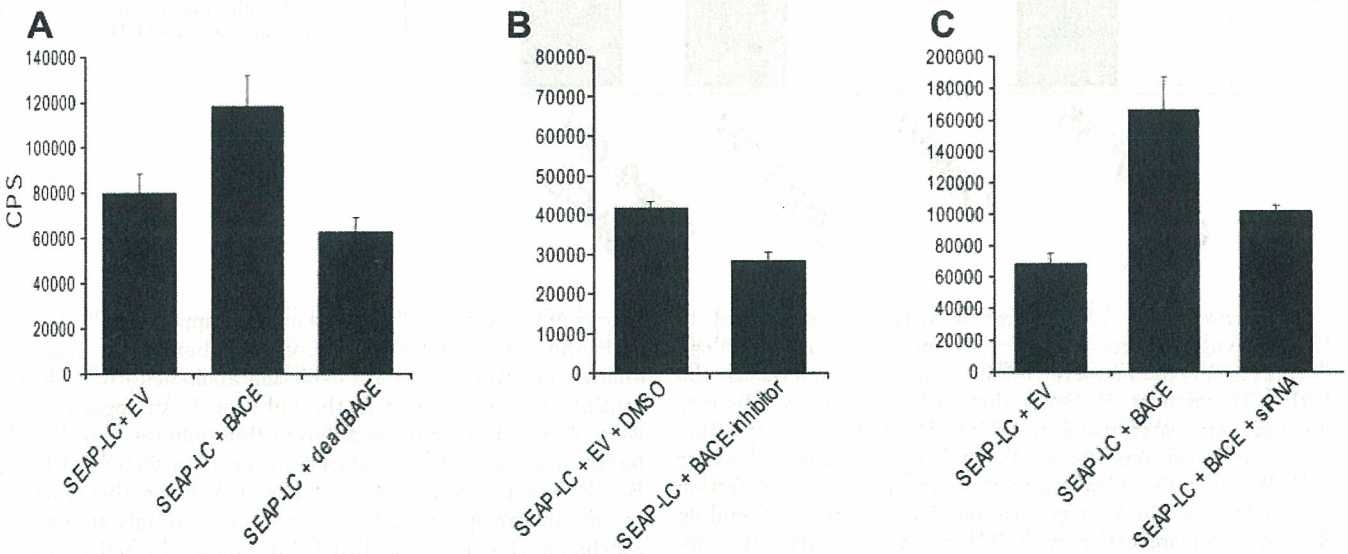

FIG. 7. **LRP shedding assay.** *A*, HEK cells were transfected with SEAP-LRP, β-galactosidase, and empty vector or with a plasmid encoding WT-BACE or a catalytically inactive BACE mutant (BACE D93/289A). *B*, HEK cells were transfected with SEAP-LRP, β-galactosidase, and empty vector and treated overnight with either Me_2SO (*DMSO*) or 12.5 μM BACE-inhibitor II. *C*, HEK cells were transfected with SEAP-LRP, β-galactosidase, and WT-BACE, and BACE-siRNA. Shown is the alkaline phosphatase activity in the conditioned medium normalized to β-galactosidase activity. Given are the means and S.D. of one of three independent assays. Both transfection and measurement were carried out in duplicate or triplicate.

when treating cells that expressed BACE at endogenous levels, indicating that the observed effect has physiologic relevance and is not restricted to cells overexpressing BACE (Fig. 7*B*). The second approach to inactivating BACE utilized siRNA-mediated silencing. Knocking down overexpressed BACE by co-transfection of BACE1-specific siRNA reduced processing of LRP by BACE (Fig. 7*C*).

LRP C-terminal Fragment (CTF) Production after BACE Co-transfection—After treatment with DAPT for 12 h we observed an increase of the LRP-CTF 25-kDa band consistent with the observations of (28) suggesting γ-cleavage of LRP. We hypothesized that, like APP, the direct substrate of γ-secretase activity would be an N-terminally cleaved form of LRP. To determine if BACE activity would produce an LRP-derived γ-secretase substrate, we co-transfected LC with BACE. This led to an increase of LRP-CTF detected by Western blot as a 25-kDa band. To confirm that this band is the substrate of γ-secretase activity, we repeated this experiment in the presence of the γ-secretase inhibitor DAPT, and detected an increased amount of the 25-kDa product. The presence of BACE further increased and co-transfection with catalytically inactive BACE mutant did not increase this band intensity (Fig. 8). These results are consistent with a BACE-mediated cleavage of LRP, generating a CTF for γ-cleavage.

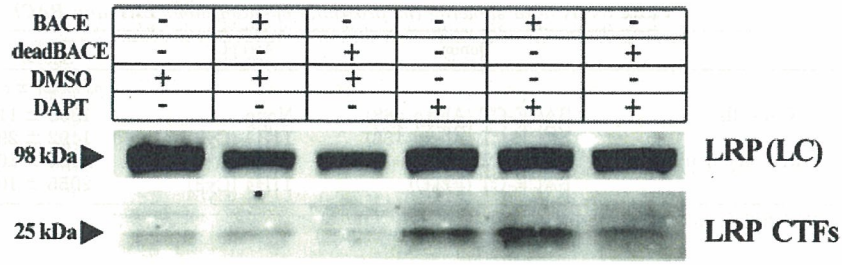

FIG. 8. **LRP CTF Western blot.** N2a cells co-transfected with LC-Myc and either empty vector, BACE, or a catalytically inactive BACE mutant (*deadBACE*) were treated with vehicle (*DMSO*) or DAPT (12 h). Increases of CTF intensity were detected after DAPT treatment and/or BACE co-transfection. Shown is the intensity of a representative blot out of four experiments without DAPT treatment and two with DAPT treatment.

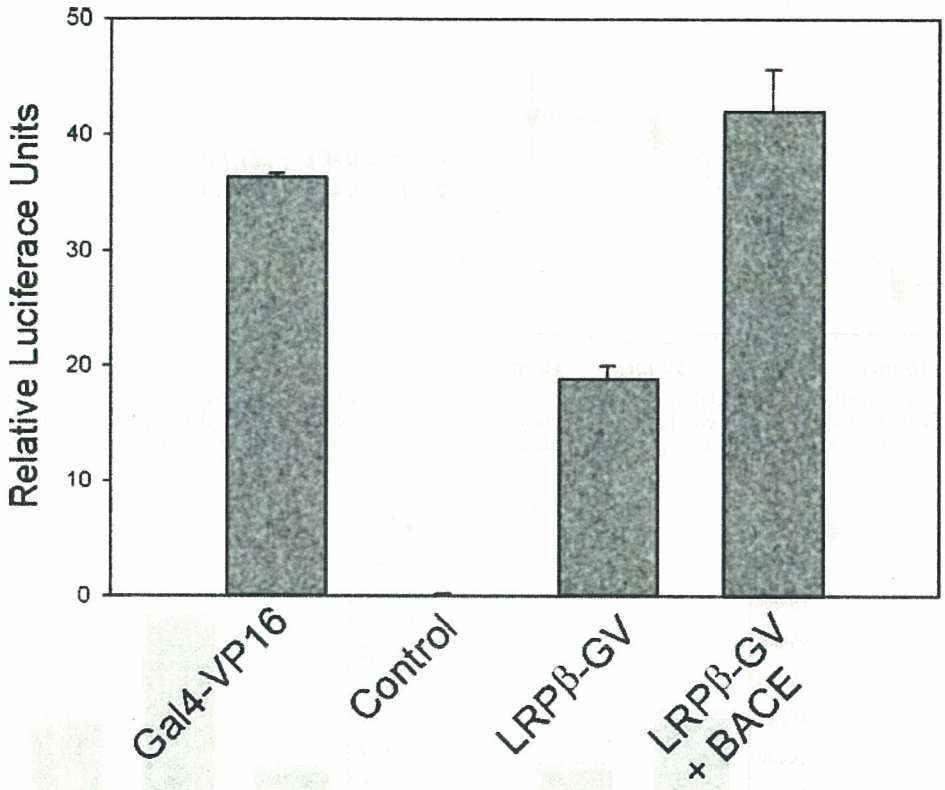

FIG. 9. **BACE increases release of LRP-ICD.** HEK293 cells were transfected with LRP-Gal4/VP16 (28) in the absence or presence of BACE, and luciferase activity determined. Activity relative to β-galactosidase is shown as the average of triplicate analyses. The addition of BACE led to a statistically significant increase in luciferase activity, suggesting that LRP undergoes BACE cleavage, and leading to subsequent release of the cytoplasmic domain and translocation to the nucleus to activate the Gal4 assay.

Luciferase Assay—LRP interaction with β-secretase leads to LRP cleavage and generation of a truncated form. By analogy to APP, it may then undergo further proteolysis and release the LRP-ICD fragment. Evidence that LRP is itself a γ-substrate has been presented using an LRP-Gal4/VP16 construct utilizing a luciferase reporter assay for LRP C-terminal cleavage (28). We used this same assay to determine if co-transfection with BACE would alter generation of this putative signaling domain. Co-transfection with BACE led to a substantial increase in luciferase activity suggesting that LRP undergoes BACE cleavage, leading ultimately to release of the cytoplasmic domain and translocation to the nucleus (Fig. 9).

DISCUSSION

In the present study, we have demonstrated that BACE interacts with the intracellular domain of LRP, a multifunctional endocytic receptor. The interaction was demonstrated by co-immunoprecipitation of BACE and LRP from overexpressing cells and from endogenous BACE and LRP in human brain samples and primary neurons. Co-localization and close proximity in both H4 and N2a cells was shown by confocal microscopy and FRET-based proximity assays, suggesting co-localization primarily in endosomes and at the cell surface. Cholesterol depletion disrupted the cell surface LRP interaction, suggesting that the interaction occurs in lipid rafts.

The FRET technique used here, FLIM, is advantageous because it provides quantitative data on protein-protein proximity with exquisite subcellular localization. The two fluorophores must be quite close (<10 nm) to support FRET; tagging LRP and BACE molecules "across the membrane" from one another or after cholesterol depletion abolishes FRET despite continued co-localization at the light level. Analogous results were obtained using three different fluorophores, multiple different antibody pairs, endogenous or transfected LRP and BACE, and two different cell types. Taken together with the co-immunoprecipitation data, our results strongly support the conclusion that LRP and BACE interact at the cell surface in raft compartments.

In contrast to γ-secretase, where at least 15 substrates have been described (44), BACE has so far appeared to be relatively specific. Sialyltransferase and PSGL-1, in addition to APP and its homologues APLP1 and 2 are the only other reported substrates of BACE (6, 43). A family of GGA adaptor proteins and the phospholipid scramblase 1 (PLSCR1) have been shown to directly interact with the BACE tail (42, 45). Interestingly, both BACE and PLSCR1 were localized in a low buoyant lipid microdomain, a potential site of interaction with APP and LRP.

In summary, our data demonstrate a close interaction of LRP and BACE in specific subcellular compartments. Although BACE and LRP are mostly co-localized in the endosomal compartments and to a lesser extent in the Golgi and on the cell surface as shown by conventional immunostaining, our FLIM data suggest that they come into closest proximity at the cell surface in lipid rafts, where it has been shown that amyloidogenic processing seems to occur in raft associated compart-

ments (13). This is in good accordance with a recent article showing that ApoE, a LRP ligand, is co-localized with APP and BACE in lipid rafts (46). Moreover, our SEAP-LC assay demonstrates that BACE-mediated cleavage of the LRP extracellular domain leads to secretion of the shed domain into the extracellular milieu. Because even the LRP165 construct (which lacks ligand binding domains and most of the extracellular part of LRP) interacts with the BACE intracellular domain and the LC-LDLR-chimera lacking the LRP intracellular domain did not interact with BACE, we postulate that the major interaction site is the intracellular domain of LRP. Whereas two candidate adaptor proteins, Fe65 and mDab, did not appear to mediate the interaction, multiple other potential adaptor proteins might either mediate or impact this interaction. Surprisingly we did not find enhancement of BACE endocytosis in LRP-null cells co-transfected with LRP. Thus, although LRP co-traffics with BACE to the cell surface, it does not appear to be critical for BACE recycling from the cell surface to endosomes. Our current data, showing an interaction between LRP and BACE, when viewed in the context of previous studies of APP-LRP interactions, suggest that LRP has a complex role in modulating APP processing. The LRP C-terminal domain also mediates an interaction with APP in similar cell compartments (22). Thus, LRP, which is highly enriched in rafts, potentially acts as a scaffolding complex in rafts for APP and for BACE; such an interaction may help explain the observations that directing APP to rafts enhances β-cleavage and Aβ generation (13).

We found that BACE activity at endogenous levels leads to an increase of secreted LRP in the medium as well as LRP-CTF, analogous to APP processing. Thus we now show that LRP is a substrate for both BACE and γ-secretase, identified as APP-processing enzymes. Whether this processing leads to a stable LRP equivalent of Aβ is unknown. Moreover BACE overexpression leads to an increase of γ-secretase-like cleavage to release LRP-ICD. Although LRP-ICD has been shown to translocate to the nucleus and interact with Fe65 and Tip60 (28, 47), whether or not it has a transcriptional role under physiological conditions remains unknown. However, both LRP (48, 49) and other members of the LDL receptor-related family (50) have been implicated as having signaling roles in neurons, and it seems likely that the cleavage of LRP we observe could modulate such signaling. Further studies will be needed to elucidate if APP and LRP act co-operatively or competitively for access to these secretases and how interactions of LRP with other ligands impact these processes.

Acknowledgments—We thank Hibiki Kawamata and Tejal Shah for assisting in the initial portion of this work. We thank the Massachusetts Alzheimer Disease Research Center Brain bank for brain samples.

REFERENCES

1. Vassar, R., Bennett, B. D., Babu-Khan, S., Kahn, S., Mendiaz, E. A., Denis, P., Teplow, D. B., Ross, S., Amarante, P., Loeloff, R., Luo, Y., Fisher, S., Fuller, J., Edenson, S., Lile, J., Jarosinski, M. A., Biere, A. L., Curran, E., Burgess, T., Louis, J. C., Collins, F., Treanor, J., Rogers, G., and Citron, M. (1999) *Science* **286,** 735–741
2. Sinha, S., Anderson, J. P., Barbour, R., Basi, G. S., Caccavello, R., Davis, D., Doan, M., Dovey, H. F., Frigon, N., Hong, J., Jacobson-Croak, K., Jewett, N., Keim, P., Knops, J., Lieberburg, I., Power, M., Tan, H., Tatsuno, G., Tung, J., Schenk, D., Seubert, P., Suomensaari, S. M., Wang, S., Walker, D., Zhao, J., McConlogue, L., and John, V. (1999) *Nature* **402,** 537–540
3. Yan, R., Bienkowski, M. J., Shuck, M. E., Miao, H., Tory, M. C., Pauley, A. M., Brashier, J. R., Stratman, N. C., Mathews, W. R., Buhl, A. E., Carter, D. B., Tomasselli, A. G., Parodi, L. A., Heinrikson, R. L., and Gurney, M. E. (1999) *Nature* **402,** 533–537
4. Hussain, I., Powell, D., Howlett, D. R., Tew, D. G., Meek, T. D., Chapman, C., Gloger, I. S., Murphy, K. E., Southan, C. D., Ryan, D. M., Smith, T. S., Simmons, D. L., Walsh, F. S., Dingwall, C., and Christie, G. (1999) *Mol. Cell Neurosci.* **14,** 419–427
5. Li, Q., and Sudhof, T. C. (2004) *J. Biol. Chem.* **279,** 10542–10550
6. Kitazume, S., Tachida, Y., Oka, R., Shirotani, K., Saido, T. C., and Hashimoto, Y. (2001) *Proc. Natl. Acad. Sci. U. S. A.* **98,** 13554–13559
7. Bennett, B. D., Denis, P., Haniu, M., Teplow, D. B., Kahn, S., Louis, J. C., Citron, M., and Vassar, R. (2000) *J. Biol. Chem.* **275,** 37712–37717
8. Capell, A., Steiner, H., Willem, M., Kaiser, H., Meyer, C., Walter, J., Lammich, S., Multhaup, G., and Haass, C. (2000) *J. Biol. Chem.* **275,** 30849–30854
9. Creemers, J. W., Ines Dominguez, D., Plets, E., Serneels, L., Taylor, N. A., Multhaup, G., Craessaerts, K., Annaert, W., and De Strooper, B. (2001) *J. Biol. Chem.* **276,** 4211–4217
10. Kinoshita, A., Fukumoto, H., Shah, T., Whelan, C. M., Irizarry, M. C., and Hyman, B. T. (2003) *J. Cell Sci.* **116,** 3339–3346
11. Huse, J. T., Pijak, D. S., Leslie, G. J., Lee, V. M., and Doms, R. W. (2000) *J. Biol. Chem.* **275,** 33729–33737
12. Riddell, D. R., Christie, G., Hussain, I., and Dingwall, C. (2001) *Curr. Biol.* **11,** 1288–1293
13. Ehehalt, R., Keller, P., Haass, C., Thiele, C., and Simons, K. (2003) *J. Cell Biol.* **160,** 113–123
14. Cordy, J. M., Hussain, I., Dingwall, C., Hooper, N. M., and Turner, A. J. (2003) *Proc. Natl. Acad. Sci. U. S. A.* **100,** 11735–11740
15. Walter, J., Fluhrer, R., Hartung, B., Willem, M., Kaether, C., Capell, A., Lammich, S., Multhaup, G., and Haass, C. (2001) *J. Biol. Chem.* **276,** 14634–14641
16. Herz, J., and Strickland, D. K. (2001) *J. Clin. Investig.* **108,** 779–784
17. Li, Y., Cam, J., and Bu, G. (2001) *Mol. Neurobiol.* **23,** 53–67
18. Kounnas, M. Z., Moir, R. D., Rebeck, G. W., Bush, A. I., Argraves, W. S., Tanzi, R. E., Hyman, B. T., and Strickland, D. K. (1995) *Cell* **82,** 331–340
19. Ulery, P. G., Beers, J., Mikhailenko, I., Tanzi, R. E., Rebeck, G. W., Hyman, B. T., and Strickland, D. K. (2000) *J. Biol. Chem.* **275,** 7410–7415
20. Pietrzik, C. U., Busse, T., Merriam, D. E., Weggen, S., and Koo, E. H. (2002) *EMBO J.* **21,** 5691–5700
21. Rebeck, G. W., Moir, R. D., Mui, S., Strickland, D. K., Tanzi, R. E., and Hyman, B. T. (2001) *Brain Res. Mol. Brain Res.* **87,** 238–245
22. Kinoshita, A., Whelan, C. M., Smith, C. J., Mikhailenko, I., Rebeck, G. W., Strickland, D. K., and Hyman, B. T. (2001) *J. Neurosci.* **21,** 8354–8361
23. Trommsdorff, M., Borg, J. P., Margolis, B., and Herz, J. (1998) *J. Biol. Chem.* **273,** 33556–33560
24. Quinn, K. A., Pye, V. J., Dai, Y. P., Chesterman, C. N., and Owensby, D. A. (1999) *Exp. Cell Res.* **251,** 433–441
25. Rozanov, D. V., Hahn-Dantona, E., Strickland, D. K., and Strongin, A. Y. (2004) *J. Biol. Chem.* **279,** 4260–4268
26. Higashi, S., and Miyazaki, K. (2003) *Biochemistry* **42,** 6514–6526
27. Kinoshita, A., Shah, T., Tangredi, M. M., Strickland, D. K., and Hyman, B. T. (2003) *J. Biol. Chem.* **278,** 41182–41188
28. May, P., Reddy, Y. K., and Herz, J. (2002) *J. Biol. Chem.* **277,** 18736–18743
29. Mikhailenko, I., Battey, F. D., Migliorini, M., Ruiz, J. F., Argraves, K., Moayeri, M., and Strickland, D. K. (2001) *J. Biol. Chem.* **276,** 39484–39491
30. von Arnim, C. A., Tangredi, M. M., Peltan, I. D., Lee, B. M., Irizarry, M. C., Kinoshita, A., and Hyman, B. T. (2004) *J. Cell Sci.* **117,** 5437–5445
31. Kao, S.-C., Krichevsky, A. M., Kosik, K. S., and Tsai, L.-H. (2004) *J. Biol. Chem.* **279,** 1942–1949
32. Berezovska, O., Frosch, M., McLean, P., Knowles, R., Koo, E., Kang, D., Shen, J., Lu, F. M., Lux, S. E., Tonegawa, S., and Hyman, B. T. (1999) *Brain Res. Mol. Brain Res.* **69,** 273–280
33. Smart, E. J., Ying, Y. S., Mineo, C., and Anderson, R. G. (1995) *Proc. Natl. Acad. Sci. U. S. A.* **92,** 10104–10108
34. Liscum, L., Arnio, E., Anthony, M., Howley, A., Sturley, S. L., and Agler, M. (2002) *J. Lipid Res.* **43,** 1708–1717
35. Orlando, L. R., Dunah, A. W., Standaert, D. G., and Young, A. B. (2002) *Neuropharmacology* **43,** 161–173
36. Berezovska, O., Ramdya, P., Skoch, J., Wolfe, M. S., Bacskai, B. J., and Hyman, B. T. (2003) *J. Neurosci.* **23,** 4560–4566
37. Bacskai, B. J., Skoch, J., Hickey, G. A., Allen, R., and Hyman, B. T. (2003) *J. Biomed. Opt.* **8,** 368–375
38. Sever, S., Damke, H., and Schmid, S. L. (2000) *J. Cell Biol.* **150,** 1137–1148
39. Abbenante, G., Kovacs, D. M., Leung, D. L., Craik, D. J., Tanzi, R. E., and Fairlie, D. P. (2000) *Biochem. Biophys. Res. Commun.* **268,** 133–135
40. Kornilova, A. Y., Das, C., and Wolfe, M. S. (2003) *J. Biol. Chem.* **278,** 16470–16473
41. Pietrzik, C. U., Yoon, I. S., Jaeger, S., Busse, T., Weggen, S., and Koo, E. H. (2004) *J. Neurosci.* **24,** 4259–4265
42. He, X., Chang, W. P., Koelsch, G., and Tang, J. (2002) *FEBS Lett.* **524,** 183–187
43. Lichtenthaler, S. F., Dominguez, D. I., Westmeyer, G. G., Reiss, K., Haass, C., Saftig, P., De Strooper, B., and Seed, B. (2003) *J. Biol. Chem.* **278,** 48713–48719
44. De Strooper, B. (2003) *Neuron* **38,** 9–12
45. Kametaka, S., Shibata, M., Moroe, K., Kanamori, S., Ohsawa, Y., Waguri, S., Sims, P. J., Emoto, K., Umeda, M., and Uchiyama, Y. (2003) *J. Biol. Chem.* **278,** 15239–15245
46. Kawarabayashi, T., Shoji, M., Younkin, L. H., Wen-Lang, L., Dickson, D. W., Murakami, T., Matsubara, E., Abe, K., Ashe, K. H., and Younkin, S. G. (2004) *J. Neurosci.* **24,** 3801–3809
47. Kinoshita, A., Whelan, C. M., Berezovska, O., and Hyman, B. T. (2002) *J. Biol. Chem.* **277,** 28530–28536
48. Bacskai, B. J., Xia, M. Q., Strickland, D. K., Rebeck, G. W., and Hyman, B. T. (2000) *Proc. Natl. Acad. Sci. U. S. A.* **97,** 11551–11556
49. Boucher, P., Liu, P., Gotthardt, M., Hiesberger, T., Anderson, R. G., and Herz, J. (2002) *J. Biol. Chem.* **277,** 15507–15513
50. Trommsdorff, M., Gotthardt, M., Hiesberger, T., Shelton, J., Stockinger, W., Nimpf, J., Hammer, R. E., Richardson, J. A., and Herz, J. (1999) *Cell* **97,** 689–701

Available online at www.sciencedirect.com
SCIENCE DIRECT®
Neuroscience Letters 402 (2006) 278–283
Neuroscience Letters
www.elsevier.com/locate/neulet

Characterization of sequential N-cadherin cleavage by ADAM10 and PS1

Kengo Uemura[a], Takeshi Kihara[b], Akira Kuzuya[c], Katsuya Okawa[a], Takaaki Nishimoto[b], Haruaki Ninomiya[d], Hachiro Sugimoto[b], Ayae Kinoshita[a,e,*,1], Shun Shimohama[c,1]

[a] *Horizontal Medical Research Organization, Kyoto University Graduate School of Medicine, Kyoto 606-8507, Japan*
[b] *Department of Neuroscience for Drug Discovery, Graduate School of Pharmaceutical Sciences, Kyoto University, Kyoto 606-8507, Japan*
[c] *Department of Neurology, Kyoto University Graduate School of Medicine, Kyoto 606-8507, Japan*
[d] *Department of Neurobiology, Tottori University Faculty of Medicine, Yonago 683-8503, Japan*
[e] *School of Health Sciences, Faculty of Medicine, Kyoto University, Kyoto 606-8507, Japan*

Received 20 March 2006; received in revised form 11 April 2006; accepted 14 April 2006

Abstract

N-cadherin is essential for excitatory synaptic contact in the hippocampus. At the sites of synaptic contact, it forms a complex with Presenilin 1(PS1) and β-catenin. N-cadherin is cleaved by ADAM10 in response to NMDA receptor stimulation, producing a membrane fragment Ncad/CTF1 in neurons. NMDA receptor stimulation also enhances PS1/γ-secretase-mediated cleavage of N-cadherin. To characterize the regulatory mechanisms of the ADAM10 and PS1-mediated cleavages, we first identified the precise cleavage sites of N-cadherin by ADAM10 and PS1/γ-secretase by producing cleavage-deficient N-cadherin mutants. Next, we found that ectodomain shedding of N-cadherin by ADAM10 is a primary regulatory step in response to calcium influx, and that it is required for the subsequent PS1/γ-secretase-mediated ε-cleavage of N-cadherin, which is a constitutive process to yield a cytoplasmic fragment, Ncad/CTF2. Since N-cadherin is essential for the structure and function of synapses including the long-term potentiation, those proteolytic events of N-cadherin should affect the adhesive behavior of the synapses, thereby taking part in learning and memory.

Keywords: Presenilin 1; N-cadherin; ADAM10; Synapse; Alzheimer's disease

Dysfunction in the synapse, especially alterations of hippocampal synaptic efficacy leads to the impairment of memory, a major symptom of Alzheimer's disease (AD) [18]. In AD, synaptic loss correlates with the severity of cognitive impairment better than senile plaques or neurofibrillary tangles [19]. In fact, loss of hippocampal synaptophysin immunoreactivity is an early pathological marker in AD [8]. Thus, investigating the regulatory mechanism of synaptic contact is important for the elucidation of AD pathogenesis.

N-cadherin, an essential molecule for synaptic contact, is abundantly localized in hippocampal synapses [2]. The cytoplasmic domain of cadherin associates with the actin cytoskeleton via β-catenin and regulates synaptic contact, synaptogenesis and dendritic spine morphology [14,20]. Recently, it was shown that the cleavage of N-cadherin by ADAM10 occurs after NMDA stimulation of neuronal cells. This cleavage results in a redistribution of β-catenin from the cell surface to the nucleus [16], indicating that cadherin-based cell-cell contact might regulate β-catenin signaling. However, the exact mechanism how ADAM10-mediated cleavage of N-cadherin affects nuclear β-catenin signaling is not known yet.

PS1, a causative gene of familial AD, is a component of γ-secretase, which cleaves β-amyloid precursor protein to generate Aβ peptides [4]. Interestingly, PS1 is located at the synapse and forms complexes with N-cadherin [5]. N-cadherin is also cleaved by PS1/γ-secretase after NMDA receptor stimulation, although the precise cleavage site has never been determined [12]. Both ADAM10- and PS1-mediated cleavages are triggered by NMDA receptor stimulation in neuron, however, whether N-cadherin cleavage by ADAM10 and PS1/γ-secretase occur 'sequentially' or 'independently' have never been clarified. Since N-cadherin is essential for the synapse structure and function, the precise mechanism of N-cadherin metabolism after neuronal excitation should be elucidated.

* Corresponding author at: Department of Health Science, Faculty of Medicine, Kyoto University, 53 Shogoinkawahara-cho, Sakyo-ku, Kyoto 606-8507, Japan. Tel.: +81 75 751 3969; fax: +81 75 751 3969.
E-mail address: akinoshita@hs.med.kyoto-u.ac.jp (A. Kinoshita).
[1] These authors equally contributed to this work.

0304-3940/$ – see front matter © 2006 Elsevier Ireland Ltd. All rights reserved.
doi:10.1016/j.neulet.2006.04.018

In this study, we have identified the precise cleavage sites of N-cadherin by ADAM10 and PS1/γ-secretase. Moreover, we revealed that the ADAM10-mediated ectodomain shedding of N-cadherin, which would disrupt cell-cell (synaptic) contact, is a prerequisite for the secondary PS1/γ-secretase cleavage. Further, we have proven that the ADAM10-mediated shedding is a regulated process in response to calcium influx via NMDA-type glutamate receptor, whereas PS1/γ-secretase cleavage is a constitutive one.

Initially, we constructed several N-cadherin mutants to identify the precise cleavage sites. A cDNA copy of human N-cadherin (Genbank no.: M34064) gene was amplified from the first strand cDNA Human fetal brain (Stratagene, CA) by a forward primer 5′-TTTTTTGCTAGCACCATGGATAAAGAACGCCAGGCC-3′, and a reverse primer, 5′-TTTTTGGGCCCTCAGCTATCACCTCCACCATA-3′ and cloned into pcDNA3.1 (+) (Invitrogen, Carlsbad, CA). For C-terminal HA tagging, a reverse primer 5′-TTTTTGGGCCCTCAGGCGTAATCTGGGACGTCGTATGGGTAGTCATCACCTCCACCATACATGTCAGCA-3′ was used. The cleavage-defective cadherin mutants (GD mutant, IRD mutant, GG mutant and ED mutant) were produced by the site-directed mutagenesis method [9]. To obtain a plasmid construct expressing Ncad(FL)-GFP, the N-cadherin was cloned into pcDNA3.1/CT-GFP-TOPO (Invitrogen). Deletion mutants of N-cadherin, having an endogenous signal peptide tagged with Flag sequence at the N-terminus were produced as follows. For Ncad(ΔN)-GFP, PCR products, amplified by two different primer sets from wild-type N-cadherin construct (5′-TTTTTTGGTACCGAGCTCGGATCCA-3′ and 5′-TTTTGGGCCCGTCCTTGTAGTCA-

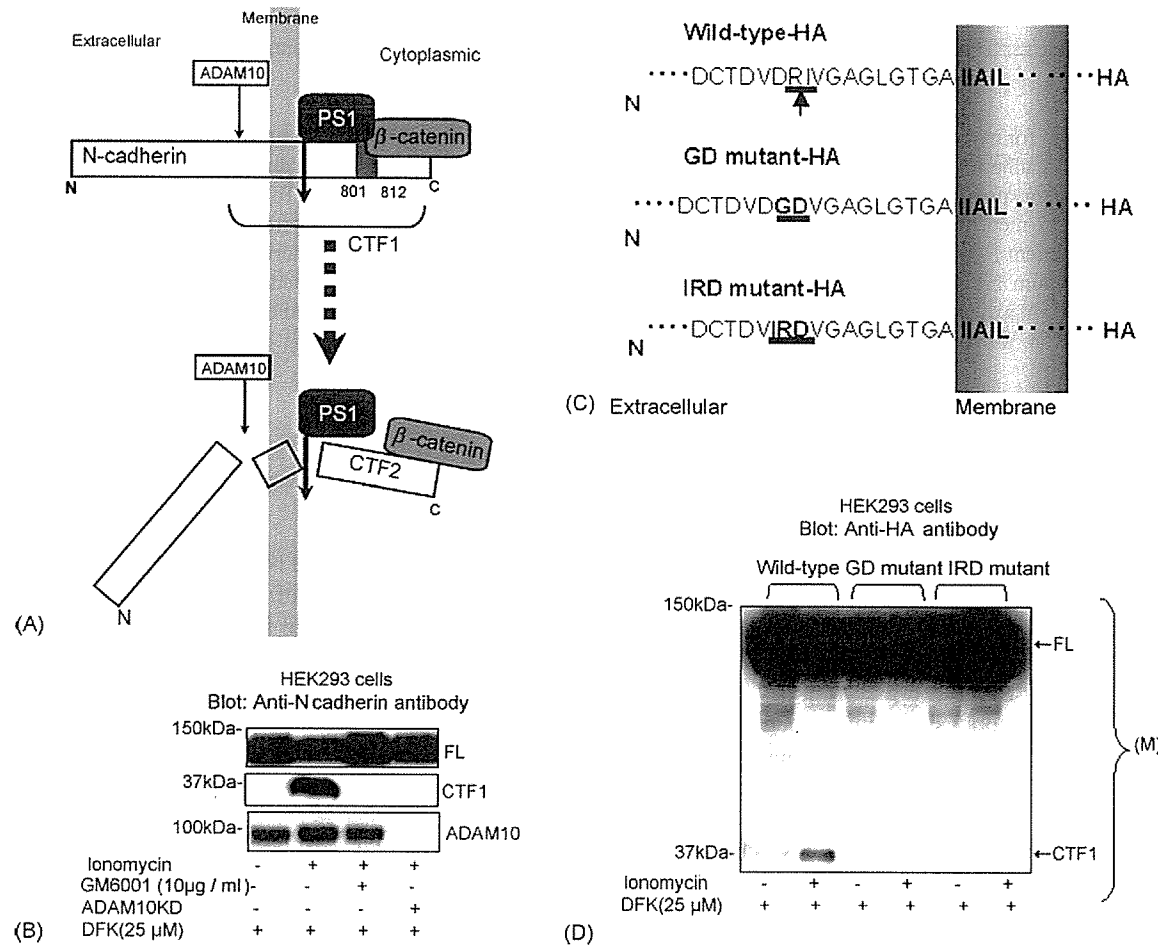

Fig. 1. ADAM10-mediated ectodomain shedding of N-cadherin. (A) A schema of N-cadherin cleavage. The N-cadherin cytoplasmic domain is linked to β-catenin. Ectodomain shedding of full-length (FL) N-cadherin by ADAM10 yields N-cadherin C-terminal fragment 1 (CTF1). N-cadherin is also cleaved at the membrane-cytosol interface by PS1/γ-secretase, leading to the release of the N-cadherin C-terminal fragment (CTF2) in the cytoplasm. Amino acids 802–819 are recognized by the anti-N-cadherin antibody, used in the present study. (B) Involvement of ADAM10 in ectodomain shedding of N-cadherin. HEK293 cells were treated by ionomycin (5 μM) for 30 min in the presence of DFK (25 μM). Total cell lysate was subjected to Western blot using anti-N-cadherin antibody. Ionomycin treatment induced ectodomain shedding, resulting in Ncad/CTF1 production, which was blocked by the presence of the metalloproteinase inhibitor, GM6001 (10 μg/ml). ADAM10 knock down (KD) also inhibited the production of Ncad/CTF1. (C) A scheme of N-cadherin mutants. Putative cleavage site was located between R^{714} and I^{715} in the extracellular domain in wild-type N-cadherin (arrow, underlined). GD mutant was created by substituting both $R^{714} \rightarrow G^{714}$ and $I^{715} \rightarrow D^{715}$ (underlined), whereas IRD mutant was made by substituting $D^{713} \rightarrow I^{713}$ and $I^{715} \rightarrow D^{715}$ (underlined). All constructs were tagged with HA at their C-terminus. (D) Both wild-type and mutant N-cadherins tagged with HA were transfected into HEK293 cells. Cells were then treated by ionomycin (5 μM) for 30 min in the presence of DFK (25 μM). Membrane fraction (M) was obtained and subjected to Western blot using anti-HA antibody. Ncad/CTF1 production was observed only in wild-type-HA transfected cells.

ACATCTTCAGGAAATCC-3′: 5′-TTTTTTGGGCCCTGCC-AGTGTGACTCCAA-3′ and 5′-TTTTTCTAGACTCGAGCG-GCCGCCA-3′) were excised by Apa I and cloned into Kpn I-Xba I sites of pcDNA 3.1(+). For Ncad(ΔEC)-GFP, different primer sets (5′-TTTTTTGGTACCGAGCTCGGAT-CCA-3′ and 5′-TTTTGGGCCCGTCCTTGTAGTCAACATC-TTCAGGAAATCC-3′: 5′-TTTTGGGCCCATCATTGCCATC-CTGCTCTGCATC-3′) were used. Then the constructs were subcloned into pcDNA3.1/CT-GFP-TOPO (Invitrogen) for C-terminal GFP-fusion. Precise cloning of all reading frame was verified by sequencing.

We used HEK293 cells for the transient transfection of the N-cadherin constructs in order to analyze the mutation and cleavage. HEK293 cells were maintained in DMEM containing 10% fetal bovine serum. The transfection was done by Lipofectamine 2000 (Invitrogen) according to the manufacturer's protocol.

To further verify the results of HEK293 cells, primary cultured cells were also used. They were obtained from the cerebral cortex of fetal mice (14–16 days gestation). Cultures were incubated in Neurobasal medium supplemented with B27 (Invitrogen).

In order to analyze the effect of ADAM10 on the cleavage, we undertook ADAM10 knock down experiments. siRNA duplexes (Stealth RNAi) were synthesized by Invitrogen.: 5′-UUUGACCCAAAUUCUUAGAUUCUCC-3′ (sense); 5′-GGAGAAUCUAAGAAUUUGGGUCAAA-3′ (antisense). Control cells were transfected with Block-it™ Fluorescent Oligo (Invitrogen). Plasmids encoding N-cadherin and its mutants as well as siRNA constructs were transfected into HEK293 cells using Lipofectamine 2000 (Invitrogen). Twenty-four hours after the transfection of siRNA, the effect of the ADAM10-knock down on the N-cadherin cleavage was analyzed.

To analyze the effect of inomycin (Calbiochem), NMDA and AMPA treatment on N-cadherin cleavage, the medium was changed to Opti-MEM I (Invitrogen) containing designated concentrations of stimulatory reagents. For the inhibition assay of N-cadherin cleavage, cells were pre-incubated with Opti-MEM I containing one of the inhibitors; difluoroketone (DFK, from Sigma) for 2 h, GM6001 (Calbiochem) for 1 h, MK801 for 30 min and then exchanged into OPTI-MEM I containing both a stimulatory and an appropriate inhibitory reagent. All of the control cells were treated by the sham medium exchange by OPTI-MEM I.

Preparation of protein samples, cell fractionation, the Western blot and immunoprecipitation analysis were carried out as described elsewhere [21]. For probing N-cadherin and ADAM10, anti-N-cadherin antibody was obtained from Transduction Laboratories, anti-ADAM10 from Chemicon. Anti-mouse and rabbit horseradish peroxidase-conjugated secondary antibodies were obtained from Amersham Biosciences. In vitro cleavage of N-cadherin was performed according to the previous report [6].

Mass spectrometric identification of proteins was performed as previously described [10]. Molecular mass analyses of triptic peptides were performed using an ultraflex TOF/TOF (Bruker Daltonics).

As shown in Fig. 1A, PS1, N-cadherin and β-catenin form a complex at the plasma membrane to stabilize synaptic contact [5]. E- and N-cadherin are cleaved by ADAM10 at the extracellular domain, yielding CTF1 at the membrane fraction [13,16]. E-cadherin is either directly, or following the metalloproteinase (ADAM10)-mediated ectodomain shedding, cleaved by PS1/γ-secretase at the membrane-cytosol interface (ε-cleavage), yielding cytoplasmic fragment Ecad/CTF2 [11]. PS1/γ-secretase-mediated cleavage of N-cadherin was subsequently reported [12] although the precise cleavage site has never been determined.

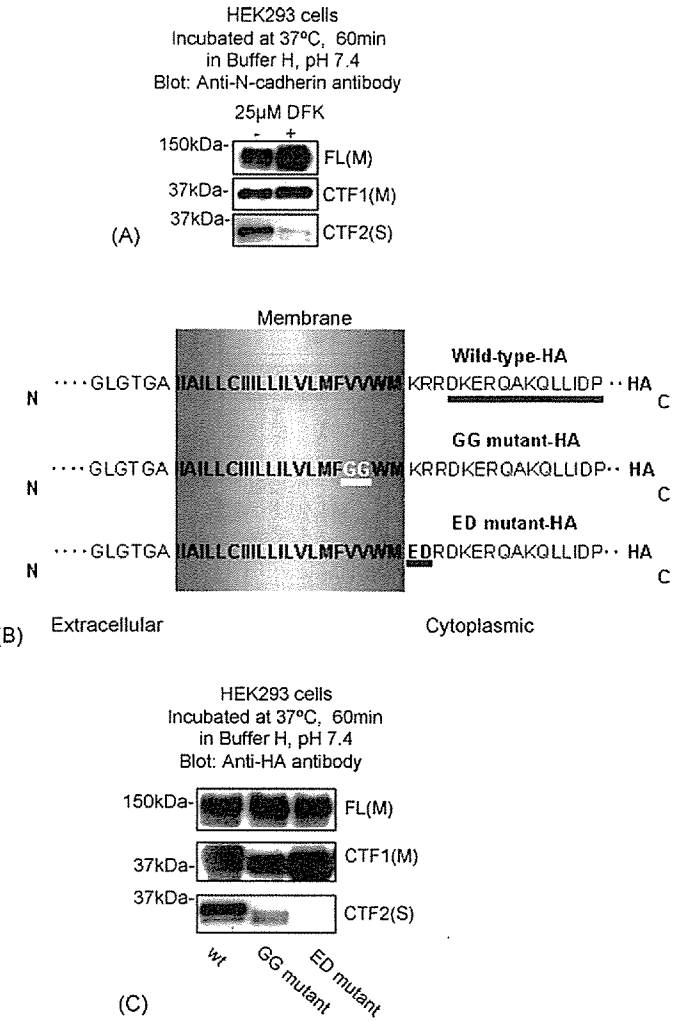

Fig. 2. PS1/γ-secretase cleaves N-cadherin at the membrane-cytosol interface. (A) The membrane fraction prepared from HEK293 cells was incubated in the presence or absence of γ-secretase inhibitor (DFK), at 37 °C, 1 h. Both membrane (M) and soluble (S) fractions were probed with anti-N-cadherin antibody. Note that the degradation of the FL N-cadherin and the production of Ncad/CTF2 are inhibited in the presence of 25 μM DFK. (B) A schema of a wt and two mutant N-cadherin constructs. GG mutant was produced by substitution of $V^{743} \rightarrow G^{743}$ and $V^{744} \rightarrow G^{744}$ (underlined). ED mutant was produced by substitution of $K^{747} \rightarrow E^{747}$ and $R^{748} \rightarrow D^{748}$ (underlined). Underline in wild-type-HA indicates the peptide sequences obtained by the MAS analysis of Ncad/CTF2. (C) The membrane fraction of transfected cells were collected and incubated in Buffer H at 37 °C for 1 h. Wild-type-HA was cleaved to yield Ncad/CTF2, as demonstrated by the Western blot using anti-HA antibody (left). The production of Ncad/CTF2 was reduced in the presence of GG mutation (middle), and completely abolished by ED mutation (right).

We first analyzed the mechanism of Ncad/CTF1 production in the presence of DFK, a γ-secretase inhibitor, to minimize the effect of PS1/γ-secretase (Fig. 1B). As reportedly, Ncad/CTF1 was produced from full-length (FL) N-cadherin in response to ionomycin treatment in the presence of DFK. Ncad/CTF1 production was inhibited by the metalloproteinase inhibitor, GM6001, or by ADAM10 knockdown, confirming that ADAM10-mediated cleavage is involved in Ncad/CTF1 production. From the homology to the cleavage sites of other ADAM10 substrates, we speculated ADAM10-mediated cleavage of N-cadherin to occur between R^{714} and I^{715} in the extracellular domain. Thus, we created two mutants: (1) GD mutant by substituting both $R^{714} \rightarrow G^{714}$ and $I^{715} \rightarrow D^{715}$, (2) IRD mutant by substituting $D^{713} \rightarrow I^{713}$ and $I^{715} \rightarrow D^{715}$ (Fig. 1C). Both GD and IRD mutations completely abolished Ncad/CTF1 production after ionomycin treatment (Fig. 1D), indicating that calcium influx triggers ADAM10-mediated ectodomain shedding of N-cadherin between R^{714} and I^{715}.

Next we wished to determine the precise cleavage mechanism of N-cadherin by PS1/γ-secretase. As reportedly, in vitro cleavage assay revealed that Ncad/CTF2 was produced by γ-secretase (Fig. 2A). In order to determine the precise cleavage site, human N-cadherin tagged with HA was transfected into HEK293 cells and subjected to in vitro cleavage. Ncad/CTF2

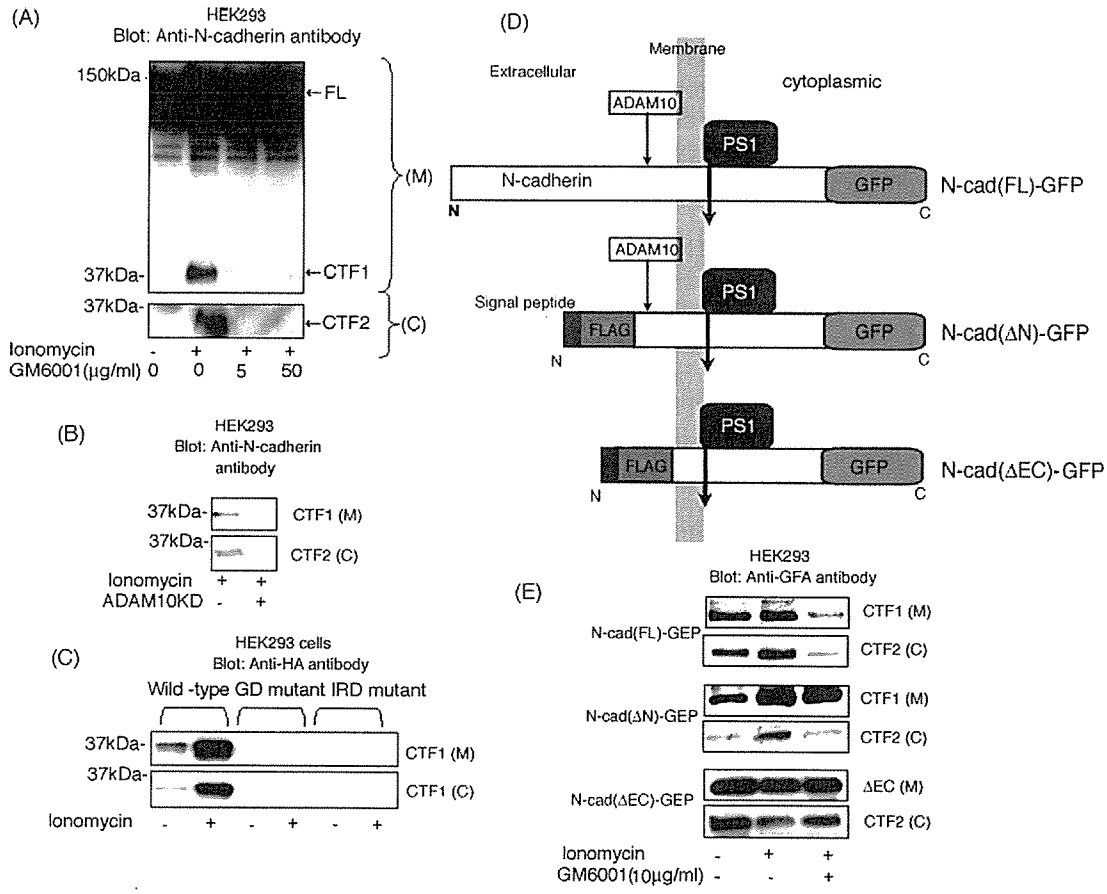

Fig. 3. ADAM10-mediated ectodomain shedding is the primary regulatory step of Ncad/CTF2 production. (A) HEK293 cells were treated by ionomycin (5 μM, 30 min) in the presence of designated concentration of GM6001. Cells were fractionated and both membrane and cytoplasmic fractions were subjected to Western blot. Ncad/CTF1 production was almost completely inhibited in the presence of 50 μg/ml GM6001 in the membrane fraction (M). Ncad/CTF2 production was observed only in the absence of GM6001 in the cytoplasmic fraction (C). (B) ADAM10 in HEK293 cells were knocked down (KD) by siRNA for 24 h. Both wild-type and ADAM10KD HEK293 cells were treated by ionomycin (5 μM, 30 min). Cells were fractionated and subjected to Western blot. Both Ncad/CTF1 and Ncad/CTF2 productions were significantly inhibited in the ADAM10 KD background. (C) N-cadherin mutants deficient in ADAM10-mediated ectodomain shedding were transfected into HEK293 cells (see Fig. 1C). Cells were treated by ionomycin (5 μM, 30 min), and both (M) and (C) fractions were subjected to Western blot using anti-HA antibody. Ncad/CTF2 production was observed only in wild-type-HA transfected cells in which abundant Ncad/CTF1 was produced. (D) A scheme of N-cadherin deletion mutants tagged with GFP. In Ncad(FL)-GFP, GFP was fused to the C-terminus of wild-type N-cadherin. In Ncad(ΔN)-GFP, the signal peptide from the wild-type N-cadherin and the Flag sequence were added to the N-terminus of putative ADAM10-mediated cleavage site of N-cadherin with GFP fusion to the C-terminus. In Ncad(ΔEC)-GFP, the signal peptide and the Flag sequence were added just N-terminus of intramembrane domain of N-cadherin, thus, Ncad(ΔEC)-GFP has no recognition site for ADAM10-mediated ectodomain shedding. (E) Effects of N-cadherin deletion on PS1/γ-secretase-mediated cleavage. N-cadherin deletion mutants were transfected into HEK293 cells. Cells were treated by ionomycin (5 μM, 30 min), in the presence or absence of GM6001 (10 μg/ml), and (M) and (C) fractions were subjected to Western blot, using anti-GFP antibody. Ionomycin treatment enhanced Ncad/CTF2 production in HEK293 cells transfected with N-cad(FL)-GFP (top) and Ncad(ΔN)-GFP plasmids (middle). Production of Ncad/CTF2 was inhibited by GM6001. In Ncad(ΔEC)-GFP transfected cells, the robust amount of Ncad/CTF2 production was seen even in the absence of ionomycin treatment. Ncad/CTF2 production was neither stimulated by ionomycin nor inhibited by GM6001 (bottom). The increase of Ncad/CTF1 production after ionomycin treatment was not clear in this experiment, possibly due to subsequent PS1/γ-secretase-mediated cleavage of Ncad/CTF1.

produced in vitro was immunoprecipitated using polyclonal anti-HA antibody (Sigma) and subjected to MAS analysis. We obtained signals from peptide sequence, 'DKERQAKQLLIDP' (indicated in Fig. 2B, wild-type-HA), which was derived from the cytoplasmic domain of N-cadherin, adjacent to the membrane-cytosol interface (data not shown). To define the cleavage sequence more precisely, we created two kinds of N-cadherin mutants (Fig. 2B). (1) GG mutant by substitution of $V^{743} \rightarrow G^{743}$ and $V^{744} \rightarrow G^{744}$ (located inside the transmembrane domain, an analogous mutant to a processing-deficient V1744K Notch mutant [17]). (2) ED mutant by substitution of $K^{747} \rightarrow E^{747}$ and $R^{748} \rightarrow D^{748}$ (located at the membrane-cytosol interface). In contrast to wtN-cadherin (Fig. 2C, left), Ncad/CTF2 production was compromised in the presence of GG mutation (Fig. 2C, middle) and abolished by ED mutation (Fig. 2C, right), indicating that human N-cadherin is cleaved by PS1/γ-secretase at the membrane-cytosol interface (ε-cleavage).

Then, we wished to determine how those two N-cadherin cleavages by ADAM10 and PS1/γ-secretase are regulated. Ncad/CTF1 production after calcium influx was inhibited by GM6001 in a dose-dependent manner (Fig. 3A, top). However, Ncad/CTF2 in the cytoplasmic fraction was observed only in the absence of GM6001, suggesting that the ectodomain shedding by ADAM10 is required for the production of Ncad/CTF2 (Fig. 3A, bottom). ADAM10 knockdown also significantly inhibited Ncad/CTF2, as well as Ncad/CTF1 production, supporting the importance of ectodomain shedding (Fig. 3B). Furthermore, it was revealed that Ncad/CTF2 was not produced in ADAM10-cleavage-deficient N-cadherin mutants (GD, IRD mutants) (Fig. 3C). Since GD and IRD mutants have intact intramembrane and cytoplasmic domains, these results confirm the requirement of precedent ectodomain shedding for PS1/γ-secretase-mediated cleavage.

To determine whether 'ectodomain shedding' is the 'primary' regulatory mechanism of Ncad/CTF2 production or, alternatively, calcium influx can also affect PS1/γ-secretase activity to promote Ncad/CTF2 production, three N-cadherin constructs were created: (1) N-cad (FL)-GFP in which GFP is fused to C-terminus of wild-type FL N-cadherin, (2) Ncad(ΔN)-GFP in which the signal peptide and Flag sequence were added to N-terminus of putative ADAM10-mediated cleavage site with GFP fusion to C-terminus, (3) Ncad(ΔEC)-GFP in which the signal peptide and Flag sequence were added just N-terminus of the intramembrane domain, thus has no recognition site for ADAM10-mediated ectodomain shedding (Fig. 3D). As expected, calcium influx enhanced Ncad/CTF2 production in both conditions transfected with either N-cadherin(FL)-GFP or Ncad(ΔN)-GFP. The production was inhibited by GM6001, thus, indicating that the amount of Ncad/CTF2 was primarily regulated at the level of ectodomain shedding, regardless of the deletion of N-terminal domain of N-cadherin (Fig. 3E, top, middle). Strikingly, in Ncad(ΔEC)-GFP transfected cells, robust amount of Ncad/CTF2 production was observed without stimulation by ionomycin, suggesting that it was constitutively produced from this construct (Fig. 3E, bottom). Collectively, these results indicate that calcium influx triggers primarily ADAM10-mediated ectodomain shedding, which then activates PS1/γ-secretase to produce Ncad/CTF2.

Previous studies demonstrated that Ncad/CTF2 was produced after the stimulation of NMDA receptor [12], and that Ncad/CTF1 production is linked to NMDA receptor stimulation [16]. Therefore, we wished to address whether the sequential cleavage is critically involved in the physiological processing of N-cadherin using primary neuronal cells (Fig. 4). The result obtained from the primary neurons confirmed that excitatory neurotransmission via NMDA receptor triggers sequential proteolysis of N-cadherin in neuronal cells (Fig. 4A and B).

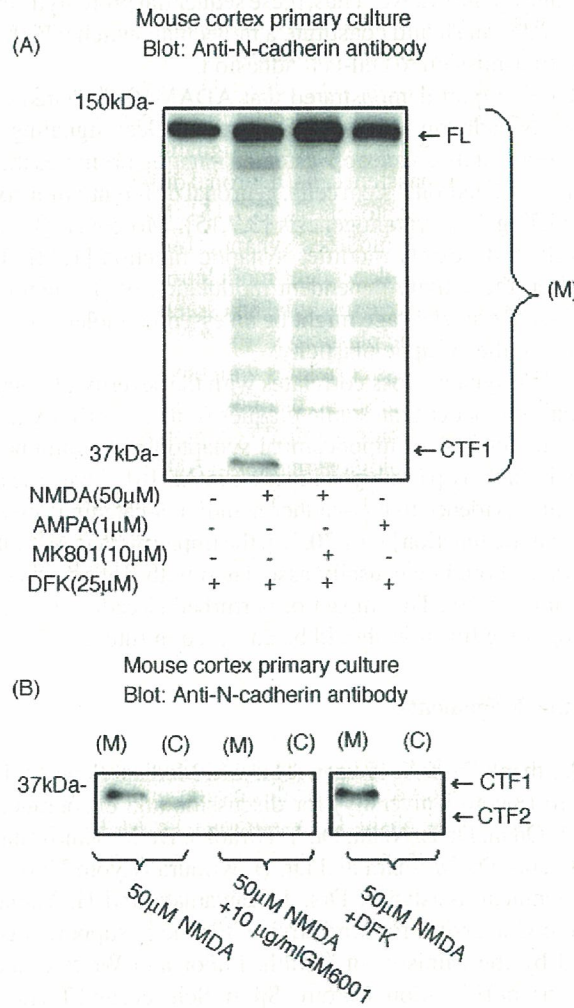

Fig. 4. NMDA-type glutamate receptor stimulation is linked to sequential proteolysis of N-cadherin in neurons. (A) Primary neurons obtained from the mouse cortex were treated by either NMDA (50 μM) or AMPA (1 μM) for 1 h in the presence of DFK (25 μM) and (M) fraction was subjected to Western blot. NMDA, but not AMPA treatment yielded Ncad/CTF1. Ncad/CTF1 production after NMDA treatment was completely inhibited by the simultaneous administration of NMDA receptor antagonist, MK801 (10 μM). (B) Primary neurons obtained from the mouse cortex were treated by NMDA (50 μM). Cells were fractionated and both (M) and (C) fractions were subjected to Western blot. NMDA treatment yielded Ncad/CTF1 in (M) fraction and Ncad/CTF2 in (C) traction. Both Ncad/CTF1 and Ncad/CTF2 productions were inhibited by GM6001 (10 μg/ml), whereas DFK (25 μM) inhibited only Ncad/CTF2 production, confirming that the secondary cleavage of N-cadherin is mediated by PS1/γ-secretase.

Previous studies demonstrated that N-cadherin undergoes the proteolytic cleavages by ADAM10 and PS1/γ-secretase in response to NMDA-type receptor-mediated calcium influx [12,16]. However, it still remains unknown how these two cleavages are regulated in the neuronal cells and the precise cleavage sites of N-cadherin were not identified yet. In the present study, we have revealed: (1) both the precise cleavage sites of human N-cadherin by ADAM10 and PS1/γ-secretase, (2) the ADAM10-mediated ectodomain shedding is a prerequisite for the subsequent PS1/γ-secretase-mediated ε-cleavage, (3) ADAM10-mediated cleavage is a regulated process in response to calcium influx, whereas PS1/γ-secretase-mediated secondary cleavage is constitutive. Thus, these sequential proteolytic events of N-cadherin should constitute a molecular switch which links neurotransmission to cell-cell adhesion.

Recent report demonstrated that ADAM10-mediated cleavage of N-cadherin enhances β-catenin nuclear signaling [16]. Developmentally, nuclear β-catenin signaling promotes the proliferation of neuronal stem cells, neuronal differentiation, axonal remodeling and synaptogenesis [3,7,15]. Moreover, β-catenin actively and flexibly modifies synaptic function [1,22]. Taken together, the activity-dependent modulation of β-catenin level via N-cadherin cleavage might be an essential molecular mechanism for the synaptic plasticity.

In AD, synaptic loss correlates with the severity of cognitive impairment better than senile plaques or neurofibrillary tangles [19]. In fact, loss of hippocampal synaptophysin immunoreactivity is an early pathological marker in AD [8]. Given the accumulating evidence that N-cadherin and/or β-catenin is essential for synaptic function [1,14,20,22], the impairment in N-cadherin cleavage should be causally associated with synaptic dysfunction in the brain. The impact of perturbed N-cadherin cleavage on cognitive function should be analyzed in future.

Acknowledgements

We thank Dr. B.T. Hyman (Harvard Medical School), Dr. Y. Kaziro (Kyoto University) for discussion and encouragement, Ms. T. Odan, Dr. E. Nishi, Dr. Y. Hiraoka, Dr. M. Kinoshita, Ms. A. Kitano, Dr. M. Ihara and Dr. H. Kimura (Kyoto University) for technical assistance, Drs. J. Kawamata and H. Yamashita (Kyoto University) for kind advice. Financial support was provided by the Ministry of Health, Labor and Welfare and the Ministry of Education, Culture, Sport, Science, and Technology of Japan, Smoking Research Foundation, Philip Morris Inc.and Philip Morris International.

References

[1] S.X. Bamji, K. Shimazu, N. Kimes, J. Huelsken, W. Birchmeier, B. Lu, L.F. Reichardt, Role of beta-catenin in synaptic vesicle localization and presynaptic assembly, Neuron 40 (2003) 719–731.

[2] D.L. Benson, H. Tanaka, N-cadherin redistribution during synaptogenesis in hippocampal neurons, J. Neurosci. 18 (1998) 6892–6904.

[3] A. Chenn, C.A. Walsh, Regulation of cerebral cortical size by control of cell cycle exit in neural precursors, Science 297 (2002) 365–369.

[4] B. de Strooper, P. Saftig, K. Craessaerts, H. Vanderstichele, G. Guhde, W. Annaert, K. Von Figura, F. Van Leuven, Deficiency of presenilin-1 inhibits the normal cleavage of amyloid precursor protein, Nature 391 (1998) 387–390.

[5] A. Georgakopoulos, P. Marambaud, S. Efthimiopoulos, J. Shioi, W. Cui, H.C. Li, M. Schutte, R. Gordon, G.R. Holstein, G. Martinelli, P. Mehta, V.L. Friedrich Jr., N.K. Robakis, Presenilin-1 forms complexes with the cadherin/catenin cell-cell adhesion system and is recruited to intercellular and synaptic contacts, Mol. Cell 4 (1999) 893–902.

[6] Y. Gu, H. Misonou, T. Sato, N. Dohmae, K. Takio, Y. Ihara, Distinct intramembrane cleavage of the beta-amyloid precursor protein family resembling gamma-secretase-like cleavage of Notch, J. Biol. Chem. 276 (2001) 35235–35238.

[7] A.C. Hall, F.R. Lucas, P.C. Salinas, Axonal remodeling and synaptic differentiation in the cerebellum is regulated by WNT-7a signaling, Cell 100 (2000) 525–535.

[8] O. Heinonen, H. Soininen, H. Sorvari, O. Kosunen, L. Paljarvi, E. Koivisto, P.J. Riekkinen Sr., Loss of synaptophysin-like immunoreactivity in the hippocampal formation is an early phenomenon in Alzheimer's disease, Neuroscience 64 (1995) 375–384.

[9] Y. Imai, Y. Matsushima, T. Sugimura, M. Terada, A simple and rapid method for generating a deletion by PCR, Nucleic Acids Res. 19 (1991) 2785.

[10] O.N. Jensen, A. Podtelejnikov, M. Mann, Delayed extraction improves specificity in database searches by matrix-assisted laser desorption/ionization peptide maps, Rapid Commun. Mass Spectrom. 10 (1996) 1371–1378.

[11] P. Marambaud, J. Shioi, G. Serban, A. Georgakopoulos, S. Sarner, V. Nagy, L. Baki, P. Wen, S. Efthimiopoulos, Z. Shao, T. Wisniewski, N.K. Robakis, A presenilin-1/gamma-secretase cleavage releases the E-cadherin intracellular domain and regulates disassembly of adherens junctions, EMBO J. 21 (2002) 1948–1956.

[12] P. Marambaud, P.H. Wen, A. Dutt, J. Shioi, A. Takashima, R. Siman, N.K. Robakis, A CBP binding transcriptional repressor produced by the PS1/epsilon-cleavage of N-cadherin is inhibited by PS1 FAD mutations, Cell 114 (2003) 635–645.

[13] T. Maretzky, K. Reiss, A. Ludwig, J. Buchholz, F. Scholz, E. Proksch, B. de Strooper, D. Hartmann, P. Saftig, ADAM10 mediates E-cadherin shedding and regulates epithelial cell-cell adhesion, migration, and beta-catenin translocation, Proc. Natl. Acad. Sci. U.S.A. 102 (2005) 9182–9187.

[14] S. Murase, E. Mosser, E.M. Schuman, Depolarization drives beta-Catenin into neuronal spines promoting changes in synaptic structure and function, Neuron 35 (2002) 91–105.

[15] J.J. Otero, W. Fu, L. Kan, A.E. Cuadra, J.A. Kessler, Beta-catenin signaling is required for neural differentiation of embryonic stem cells, Development 131 (2004) 3545–3557.

[16] K. Reiss, T. Maretzky, A. Ludwig, T. Tousseyn, B. de Strooper, D. Hartmann, P. Saftig, ADAM10 cleavage of N-cadherin and regulation of cell-cell adhesion and beta-catenin nuclear signalling, EMBO J. 24 (2005) 1762.

[17] E.H. Schroeter, J.A. Kisslinger, R. Kopan, Notch-1 signalling requires ligand-induced proteolytic release of intracellular domain, Nature 393 (1998) 382–386.

[18] D.J. Selkoe, Alzheimer's disease is a synaptic failure, Science 298 (2002) 789–791.

[19] R.D. Terry, E. Masliah, D.P. Salmon, N. Butters, R. DeTeresa, R. Hill, L.A. Hansen, R. Katzman, Physical basis of cognitive alterations in Alzheimer's disease: synapse loss is the major correlate of cognitive impairment, Ann. Neurol. 30 (1991) 572–580.

[20] H. Togashi, K. Abe, A. Mizoguchi, K. Takaoka, O. Chisaka, M. Takeichi, Cadherin regulates dendritic spine morphogenesis, Neuron 35 (2002) 77–89.

[21] K. Uemura, N. Kitagawa, R. Kohno, A. Kuzuya, T. Kageyama, K. Chonabayashi, H. Shibasaki, S. Shimohama, Presenilin 1 is involved in maturation and trafficking of N-cadherin to the plasma membrane, J. Neurosci. Res. 74 (2003) 184–191.

[22] X. Yu, R.C. Malenka, Beta-catenin is critical for dendritic morphogenesis, Nature Neurosci. 6 (2003) 1169–1177.

Available online at www.sciencedirect.com
SCIENCE DIRECT
ELSEVIER
Biochemical and Biophysical Research Communications 345 (2006) 951–958
BBRC
www.elsevier.com/locate/ybbrc

Activity-dependent regulation of β-catenin via ε-cleavage of N-cadherin

Kengo Uemura [a], Takeshi Kihara [b], Akira Kuzuya [c], Katsuya Okawa [a], Takaaki Nishimoto [b], Haruhiko Bito [d], Haruaki Ninomiya [e], Hachiro Sugimoto [b], Ayae Kinoshita [a,f,*,1], Shun Shimohama [c,1]

[a] *Horizontal Medical Research Organization, Kyoto University Graduate School of Medicine, Kyoto 606-8507, Japan*
[b] *Department of Neuroscience for Drug Discovery, Graduate School of Pharmaceutical Sciences, Kyoto University, Kyoto 606-8507, Japan*
[c] *Department of Neurology, Kyoto University Graduate School of Medicine, Kyoto 606-8507, Japan*
[d] *Department of Neurochemistry, The University of Tokyo, Graduate School of Medicine, Tokyo 113-8654, Japan*
[e] *Department of Neurobiology, Tottori University Faculty of Medicine, Yonago 683-8503, Japan*
[f] *Department of Health Science, Faculty of Medicine, Kyoto University, Kyoto 606-8507, Japan*

Received 18 April 2006
Available online 6 May 2006

Abstract

N-cadherin is essential for excitatory synaptic contact in the hippocampus. Presenilin 1 (PS1) is located at sites of synaptic contact, forming a complex with N-cadherin and β-catenin. Here, we report that human N-cadherin is cleaved by PS1/γ-secretase in response to physiological concentration of glutamate (Glu) stimulation, yielding a fragment Ncad/CTF2. The expression of Ncad/CTF2 in neuronal cells led to its translocation to the nucleus, and caused a prominent enhancement of cytoplasmic and nuclear β-catenin levels in a cell–cell contact dependent manner, via following mechanisms: 1, inhibition of β-catenin phosphorylation; 2, transactivation of β-catenin; and 3, inhibition of N-cadherin transcription, and finally enhanced β-catenin nuclear signaling. Since the regulation of cellular β-catenin level is essential for synaptic function, disruption in the cleavage of N-cadherin may be causally linked to the synaptic dysfunction associated with Alzheimer's disease (AD).

Keywords: Alzheimer's disease; N-cadherin; Presenilin 1; Synapse; β-Catenin

Synapses are the structures for the contacts that enable neurons to interact. N-cadherin, an essential adhesion molecule for synaptic contact, is abundantly localized in hippocampal glutamatergic synapses [1,2]. The cytoplasmic domain of cadherins associates with β-catenin and regulates cell–cell adhesion, synaptogenesis, and dendritic spine morphology [3,4].

On the other hand, β-catenin is a mediator of β-catenin nuclear signaling which regulates axonal remodeling and synaptogenesis in neurons [5]. In the absence of Wnt ligands, β-catenin is rapidly phosphorylated by glycogen synthase kinase-3β (GSK-3β) which targets β-catenin for degradation [6]. The presence of Wnt ligands inhibits GSK-3β, leading to increased cytoplasmic β-catenin levels. The accumulated β-catenin forms nuclear complexes with TCF family of transcription factors [7] and regulates expression of various genes such as cyclin D1 [8]. β-Catenin is important for synapse function [9,10]. However, we have limited information as to the mechanism through which neuronal cells control the cellular β-catenin level.

Presenilin 1 (PS1), a causative gene of familial AD (FAD), is a component of γ-secretase complex. The γ-secretase complex is essential for the cleavage of β-amyloid precursor protein to generate Aβ peptides [11]. PS1/γ-secretase complex is also involved in the ε-cleavage of several other type-I membrane proteins [12–15]. ε-Cleavage of membranous proteins releases their intracellular domains (ICDs) into the cytoplasm, most of which translocate to the nucleus and modify cellular signaling processes [16,17].

* Corresponding author. Fax: +81 75 751 3969.
E-mail address: akinoshita@hs.med.kyoto-u.ac.jp (A. Kinoshita).
[1] These authors equally contributed to this work.

0006-291X/$ - see front matter © 2006 Elsevier Inc. All rights reserved.
doi:10.1016/j.bbrc.2006.04.157

In fact, PS1 is located at the synapse and forms complexes with N-cadherin in the brain [18]. N-cadherin is cleaved by PS1/γ-secretase complex after NMDA receptor stimulation [19]. The ICDs, N-cadherin C-terminal fragment 2 (Ncad/CTF2), inhibit CBP-mediated transcription [19]. Given that cognitive decline in AD is correlated to the degree of synaptic loss [20], it is plausible that dysregulation of PS1-dependent synaptic proteins may be the earliest pathological event in AD.

Here, we report that human N-cadherin cleavage product by PS1/γ-secretase, Ncad/CTF2, translocates to the nucleus and promotes accumulation of cellular β-catenin, leading to the enhancement of β-catenin nuclear signaling. This model suggests that activity-dependent cleavage of N-cadherin by γ-secretase may modify the synaptic junctions in the neuronal system, thus playing a role in the remodeling of synapses.

Materials and methods

Plasmid constructs. For tetracycline-inducible expression of Ncad/CTF2, the cytoplasmic region (from amino acids No. 747 to No. 906 (Swiss-Prot: P19022)) of human N-cadherin was amplified from first strand cDNA Human fetal brain (Stratagene) by PCR, using a forward primer plus Kozak sequence with additional methionine in the beginning, 5′-TTTTTGGTACCATGAAACGCCGGGATAAAG-3′, and a reverse primer, 5′-TTTTTGGGCCCTCAGCTATCACCTCCACCATA-3′. The PCR product was cloned into *KpnI–ApaI* sites of pcDNA 4/TO (Invitrogen).

Cell culture and transfection. SH-SY5Y cells were maintained in DMEM containing 10% fetal bovine serum. SH-SY5Y cell lines, stably expressing wild-type (wt), P117L, and D385A PS1, were described previously [21]. For the establishment of cell lines in which Ncad/CTF2 expression can be induced by tetracycline (CTF2-tet cells), SH-SY5Y cells were first transfected with pcDNA6/TR (Invitrogen), using Lipofectamine 2000 (Invitrogen). After selection of cells by 5 μg/ml blasticidin, stably transfected clones were then transfected with Ncad/CTF2/pcDNA4/TO, and selected by 100 μg/ml zeocin. For the induction of Ncad/CTF2 expression, the medium was exchanged into DMEM, containing 1 μg/ml tetracycline (Invitrogen).

Primary cultured cells were obtained from the cerebral cortex or hippocampus of fetal rats (17–19 days gestation). Cultures were incubated in EMEM supplemented with 10% fetal calf serum or 10% horse serum.

Antibodies and chemical reagents. Anti-N-cadherin, anti-cyclin D1, and anti-total β-catenin are from Transduction Laboratories. Anti-β-tubulin is from Sigma. Anti-Phospho-β-catenin (Ser 33/37/Thr 41) is from Cell Signaling Technology. Anti-PS1 is from Santa Cruz. Alexa Fluor 546 goat anti-mouse IgG, Alexa Fluor 488 goat anti-rabbit IgG, and Alexa Fluor 430 goat anti-rabbit IgG, Alexa Fluor 514 goat anti-mouse IgG are obtained from Molecular Probe. Anti-mouse and rabbit horseradish peroxidase-conjugated secondary antibodies are from Amersham Biosciences. γ-Secretase inhibitor, difluoroketone (DFK) is from Sigma. Blasticidin, tetracycline, and zeocin, from Invitrogen. L-Glutamic acid monosodium salt, DAPI, and MK801 maleate from Nakalai tesque, Japan. Ionomycin and BAPTA-AM from Calbiochem.

Western blot and immunoprecipitation. Preparation of protein samples, the Western blot, and immunoprecipitation analysis were carried out as described elsewhere [22]. For some experiments, cells were fractionated as previously described [22].

Immunostaining. The samples for immunostaining were prepared as described elsewhere [22]. The samples were examined using a laser scanning confocal microscopy, LSM 510 META (Zeiss) or a fluorescence microscopy, Axiovert 200 (Zeiss). FRET measurement was done by a photobleaching method, which was described previously [23] (See also Supplementary Materials and methods).

Results and discussion

N-cadherin is cleaved by γ-secretase activity in SY-SY5Y cells

PS1, N-cadherin, and β-catenin form a complex at the plasma membrane to stabilize synaptic contact [18]. N-cadherin is cleaved by ADAM10 and PS1/γ-secretase in response to NMDA receptor-mediated calcium influx [19,24]. We have previously demonstrated that ADAM10 and PS1/γ-secretase 'sequentially cleave' human N-cadherin to yield a fragment, Ncad/CTF2 [25] (Fig. 1A). First, we wished to determine the relevance of Ncad/CTF2 production in our experimental system. Native SH-SY5Y cells treated with physiological concentration of Glu (10 μM) were fractionated into membrane and cytoplasmic fractions. Ncad/CTF2 in the cytoplasmic fraction progressively increased with time (Fig. 1B, 1st). Treatment of cells with 10 μM ionomycin, an agent that stimulates calcium influx, also increased Ncad/CTF2 production (Fig. 1B, 2nd). Ncad/CTF2 production was completely blocked by BAPTA-AM, an intracellular calcium chelator (Fig. 1B, 3rd). In the presence of 1 μM MK801, a NMDA receptor antagonist, Ncad/CTF2 (Fig. 1B, 4th) was hardly detectable, indicating NMDA receptor stimulation was required for the cleavage. Collectively, Ncad/CTF2 production was stimulated by NMDA receptor-mediated calcium influx in our system as well. Next, we examined the effect of PS1/γ-secretase activity on this cleavage. SH-SY5Y cells stably transfected with either wild-type PS1 (wtPS1) or dominant-negative PS1 (D385A) were treated by 10 μM Glu (Fig. 1C). D385A PS1 mutation has no γ-secretase activity [26]. After Glu treatment of wtPS1 cells, the release of Ncad/CTF2 was enhanced, compared to the native cells (Fig. 1C, 1st and 2nd). Conversely, in D385A cells, the Ncad/CTF2 production was blocked (Fig. 1C, 3rd). Similarly, γ-secretase inhibitor DFK (25 μM) reduced Ncad/CTF2 (Fig. 1C, 4th). Finally, we tested the effect of PS1 mutation linked to FAD [27] on N-cadherin cleavage. Stable expression of P117L PS1 prevented Glu-induced cleavage of N-cadherin (Fig. 1C, 5th), which is in line with the previous report [19].

Ncad/CTF2 translocates to the nucleus, and then leads to the nuclear translocation of β-catenin

We previously defined the precise cleavage site of N-cadherin by PS1/γ-secretase to be located at the membrane–cytosol interface [25]. To examine the effect of Ncad/CTF2 production in neuronal cells, we constructed a cell line (CTF2-tet cells), in which expression of N-cadherin cytoplasmic fragment (Ncad/CTF2) can be induced by tetracycline treatment (tet-on). The expression of Ncad/CTF2 after 1 μg/ml tetracycline treatment was verified by Western blot (Fig. 2A). In the absence of tetracycline, endogenous N-cadherin was observed only at the sites of cell–cell contact (Fig. 2B, left arrows). Strikingly, Ncad/CTF2

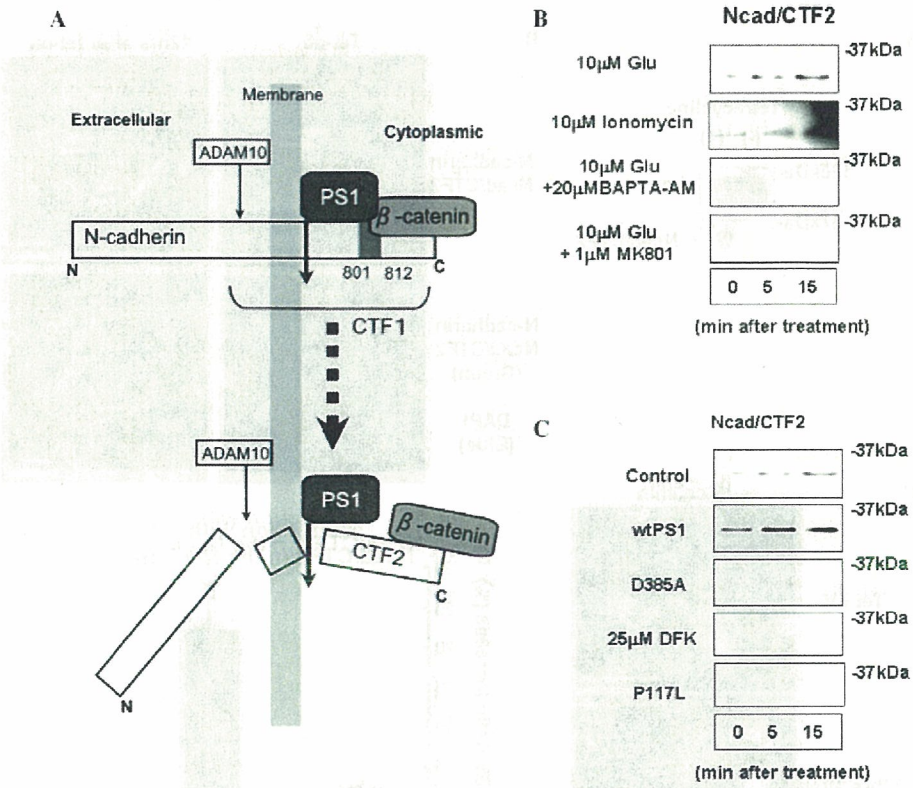

Fig. 1. N-cadherin is cleaved by γ-secretase activity in SY-SY5Y cells. (A) A schema of N-cadherin cleavage. N-cadherin cytoplasmic domain is linked to β-catenin. Ectodomain shedding by ADAM10 produces N-cadherin C-terminal fragment 1 (CTF1). CTF1 is cleaved at the membrane–cytosol interface by PS1/γ-secretase, leading to the release of the N-cadherin C-terminal fragment 2 (CTF2) in the cytoplasm. Amino acids 802–819 are the immunogenic region recognized by the anti-N-cadherin antibody. (B) Native SH-SY5Y cells were treated by Glu (10 μM) or ionomycin (10 μM). Treatment of cells by Glu (1st) or ionomycin (2nd) led to increase of Ncad/CTF2 in the cytoplasmic fraction after treatment. The production of Ncad/CTF2 after Glu treatment was diminished in the presence of 20 μM BAPTA-AM (3rd). Stimulation of cells by Glu in the presence of MK801 led to the inhibition of Ncad/CTF2 production (4th). (C) Release of Ncad/CTF2 was increased in wtPS1 cells (2nd), compared to control cells (1st). In D385A cells, production of Ncad/CTF2 was abolished (3rd). Combined treatment of native cells with Glu and DFK led to the inhibition of Ncad/CTF2 production (4th). P117L cells failed to produce Ncad/CTF2 after Glu treatment (5th).

signal was observed predominantly in the nucleus 12 h after tet-on (Fig. 2B, right arrowheads), which is in line with the localization of the other γ-secretase cleavage products [16]. Next, we examined the impact of Ncad/CTF2 expression on subcellular distribution of β-catenin. In the absence of Ncad/CTF2 expression, β-catenin was confined to cell–cell contact sites (Fig. 2C, top arrows). Twenty-four hours after tet-on, there was a striking increase in the cytoplasmic and nuclear β-catenin (Fig. 2C, bottom arrowheads). To examine the interactions between Ncad/CTF2 and β-catenin in the nuclei of the CTF2-tet cells, we utilized fluorescence resonance energy transfer (FRET) technique (Fig. 2D). FRET ratio increase after photobleaching of acceptor molecule (β-catenin) was $22.3 \pm 4.0\%$ (mean ± SD, $n = 10$), which was significantly higher than that of the control samples (between histone H1 and Ncad/CTF2; $1 \pm 1.5\%$, $n = 10$, $p < 0.0001$). PS1-dependent cleavage of membrane proteins releases their ICDs, which translocate to the nucleus [16,28]. FRET data showed a close interaction between Ncad/CTF2 and β-catenin in the nucleus, indicating that Ncad/CTF2 may directly mediate the nuclear translocation of β-catenin. Indeed, recent report demonstrated that the ectodomain shedding of N-cadherin by ADAM10 resulted in a redistribution of β-catenin from the cell surface to the nucleus [24], supporting our observation. We verified the nuclear localization of Ncad/CTF2 and β-catenin by transient transfection of Ncad/CTF2 into HEK293 cells, obtaining the same results (Supplementary Fig. 1A and C).

Cellular β-catenin level increases after Ncad/CTF2 expression

To examine the changes in β-catenin metabolism after Ncad/CTF2 expression, CTF2-tet cells, before and 24 h after tet-on, were fractionated into the cytoplasmic and the nuclear fractions, and subjected to the immunoblot analysis, using anti-total-β-catenin and anti-phospho-specific (Ser33/37/Thr41) β-catenin antibodies. Strikingly, both the cytoplasmic and the nuclear β-catenin level increased after tet-on. Conversely, β-catenin phosphorylation was suppressed following tet-on (Fig. 3A). Since Ser33/37/Thr41 phosphorylation by GSK3β subjects β-catenin to degradation, this result suggests that the inhibition of GSK3β may be involved in the accumulation of β-catenin. The accumulation of β-catenin after Ncad/CTF2

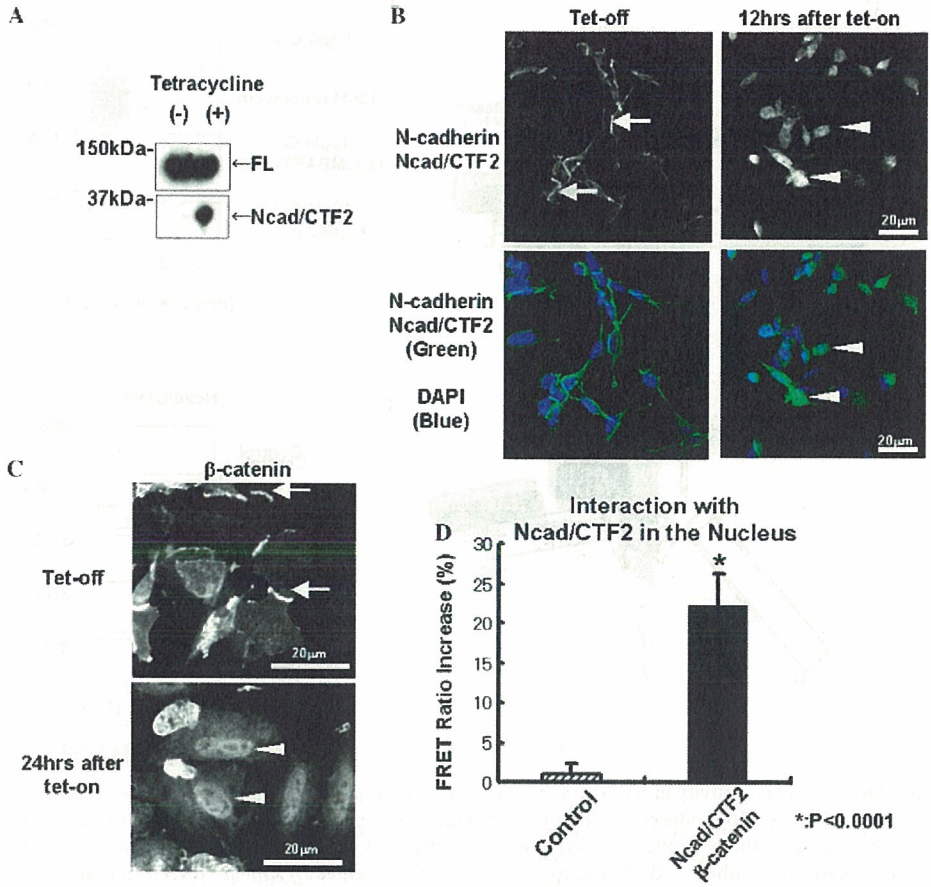

Fig. 2. Overexpression of CTF2 leads to the nuclear translocation of β-catenin. (A) CTF2-tet cells were treated by tetracycline for 24 h. Total cell lysates were subjected to Western blots using anti-N-cadherin antibody. Note that robust expression of Ncad/CTF2 was induced by tetracycline. (B) In the absence of tetracycline, N-cadherin signal was detected only at the sites of cell–cell contact with anti-N-cadherin antibody (left top arrows), thus showed no co-localization with DAPI signals (left bottom). Twelve hours after tet-on, Ncad/CTF2 immunoreactivity became prominent in the nuclei (right arrowheads), showing co-localization with DAPI signals (right bottom). Scale bar, 20 μm. (C) In the absence of tetracycline (top), β-catenin signal was localized to the sites of cell–cell contact (top arrows). 24 h after tet-on, a robust upregulation of the β-catenin level was seen, with its signals localized to the nucleus (bottom arrowheads). Scale bar, 20 μm. (D) The results of FRET. FRET ratio increase between Ncad/CTF2 and β-catenin after photobleaching was 22.3 ± 4.0% (mean ± SD, $n = 10$), which was significantly higher than that of the control samples (between histone H1 and Ncad/CTF2; 1 ± 1.5%, $n = 10$, $p < 0.0001$).

expression was verified by the experiments using HEK 293 cells (Supplementary Fig. 1B).

We examined the time course of N-cadherin and β-catenin transcription both in the mRNA and protein levels. Ncad/CTF2 transcription occurred as early as 6 h after tet-on (Fig. 3B, left top), and was followed by the increase in the amount of protein (Fig. 3B, right top). Interestingly, the transcription of full-length (FL) N-cadherin (Fig. 3B, left 2nd lane) was inhibited after 12 h, which is reflected by the level of the FL protein (Fig. 3B, right 2nd lane). In contrast to N-cadherin, β-catenin transcription increased 24 h after tet-on (Fig. 3B, left 3rd lane), whereas the enhancement of protein level was observed as early as 6 h after tet-on (Fig. 3B, right 3rd lane), indicating that mechanisms other than the transactivation were involved in the increase of β-catenin protein level in the early phase. Indeed, the inhibition of phosphorylation occurred as early as 6 h after tet-on (Fig. 3B, right 4th lane). Furthermore, the protein level of cyclin D1, a representative target protein of β-catenin nuclear signaling, increased 6 h after tet-on (Fig. 3B, right 5th lane), suggesting the activation of β-catenin nuclear signaling pathway. The upregulation of β-catenin mRNA (Fig. 3D, left) and downregulation of FL N-cadherin mRNA (Fig. 3D, right) were statistically significant. (paired t-test, $p = 0.014$ for β-catenin, $n = 3$, $p = 0.002$ for N-cadherin, $n = 3$).

Thus, Ncad/CTF2 expression leads to the accumulation of cytoplasmic β-catenin via three distinct mechanisms. The first mechanism was the inhibitory effect on the GSK3β-mediated phosphorylation of β-catenin. The second mechanism was the enhancement of β-catenin transcription. The third mechanism was the suppression of N-cadherin transcription. A reduction in the level of FL N-cadherin would decrease the membrane-tethered pool of β-catenin, which in turn would lead to the cytoplasmic accumulation of β-catenin. From the viewpoint of 'effective activation of β-catenin nuclear signaling', these three mechanisms act synergistically, enhancing the accumulation of free cytoplasmic β-catenin which can enter the nucleus as an active molecule.

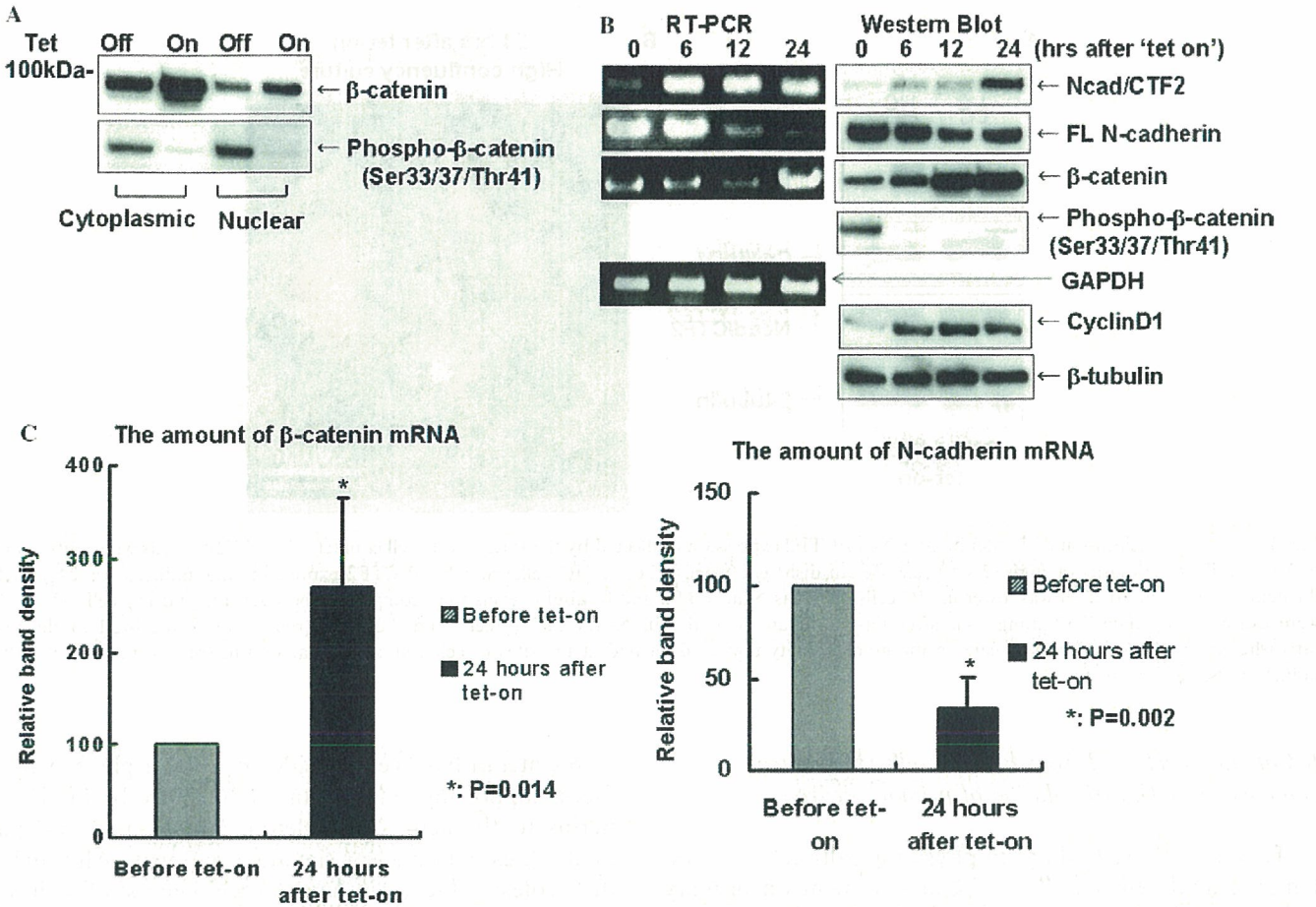

Fig. 3. Both inhibition of β-catenin phosphorylation and transcriptional activation of β-catenin are induced by N-cadherin/CTF2. (A) CTF2-tet cells were treated with tetracycline for 24 h, fractionated into cytoplasm and nucleus, and probed with anibodies against total or phospho-β-catenin (Ser33/37/Thr41). The protein level of total β-catenin increased after tet-on, both in the cytoplasmic and nuclear fractions (top). In contrast, phosphorylation of β-catenin (Ser33/37/Thr41) was inhibited in the cytoplasmic as well as in the nuclear fraction after tet-on (bottom). (B) Ncad/CTF2 transcription was observed 6 h after tet-on (left top), and was followed by an increase in the amount of protein (right top). Transcription of FL N-cadherin (left 2nd) was inhibited 12 h after tet-on, which is reflected by the reduction of protein (right 2nd). β-Catenin transcription became enhanced 24 h after tet-on (left 3rd), whereas the increase in the level of protein occurred as early as 6 h after tet-on (right 3rd). Inhibition of phosphorylation occurred 6 h after tet-on (right 4th). The protein level of cyclin D1 increased 6 h after tet-on (right 5th). The bottom lanes show the controls, the amplification of GAPDH mRNA (left bottom) and protein level of β-tubulin (right bottom), remaining unchanged. (C) The mRNA amount of β-catenin or N-cadherin was normalized by that of the control gene (GAPDH). The amount of β-catenin mRNA was significantly increased 24 h after tet-on ($n = 3$, $p = 0.014$). The N-cadherin mRNA was significantly decreased 24 h after tet-on ($n = 3$, $p = 0.002$). Data were means ± SD of three independent experiments.

Nuclear translocation and upregulation of β-catenin after Ncad/CTF2 expression is dependent on the state of cell–cell contact

Since β-catenin is an essential component of cadherin-based cell–cell contact we next asked whether the state of cell–cell contact affects the upregulation and nuclear translocation of β-catenin after Ncad/CTF2 expression. CTF2-tet cells were cultured in low or high confluency (LC or HC cells) and Ncad/CTF2 expression was induced by tet-on for 24 h. The magnitude of β-catenin and cyclin D1 upregulation was higher in LC cells, whereas the level of Ncad/CTF2 expression was comparable between LC and HC cells (Fig. 4A). Immunostaining revealed that in aggregated cells, in which extensive cell–cell adhesion was observed, nuclear translocation of β-catenin was not induced (Fig. 4B, arrow), whereas in isolated cells, Ncad/CTF2 and β-catenin were co-localized to the nucleus (Fig. 4B, arrowhead), indicating that cell–cell contact is a strong 'membrane-tethering signal' of β-catenin [24,29]. We further verified these findings by culturing CTF2-tet cells in an environment in which cells are prone to make aggregations (Supplementary Fig. 2). Thus, it is assumed that cleavage of N-cadherin would loosen cell–cell contact, and reduce contact-mediated 'tethering signal.' Interestingly, our result showed that the N-cadherin gene itself is one of the targets for transcriptional suppression by Ncad/CTF2 (Fig. 3), suggesting that Ncad/CTF2 promotes the efficient cell–cell dissociation, which could enhance β-catenin signaling by decreasing the 'tethering signal'. Collectively, the magnitude of β-catenin nuclear signaling may be determined by the balance between cell–cell contact (membrane tethering signal for β-catenin) and the production of Ncad/CTF2 (a 'mediator' of nuclear translocation).

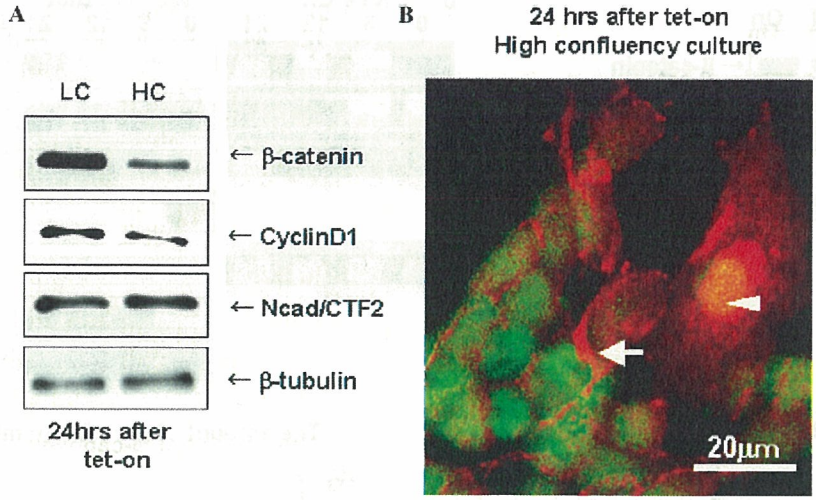

Fig. 4. Nuclear translocation of β-catenin after Ncad/CTF2 expression is affected by the state of cell–cell contact. (A) CTF2-tet cells were cultured in low (0.5×10^6cells/ϕ6 cm dish) or high (2×10^6cells/ϕ6 cm dish) confluency (LC or HC cells) and Ncad/CTF2 expression was induced for 24 h. Cellular β-catenin and cyclin D1 level was lower in HC cells, whereas Ncad/CTF2 and β-tubulin levels were comparable between LC and HC cells. (B) HC cells were examined by immunostaining 24 h after tet-on. In an isolated cell, NcadCTF2 (green) and β-catenin (red) were co-localized to the nucleus (arrowhead). In clusterized cells, β-catenin immunoreactivity remained located at the sites of cell–cell contact (arrow) in spite of nuclear Ncad/CTF2 induction. Scale bar, 20 μm.

β-Catenin is released from PS1/N-cadherin/β-catenin complex after Glu stimulation of primary neurons

To verify above findings in physiologically relevant system, we analyzed the effect of Glu treatment on primary neuron obtained from rat cortex. By fractionating neurons after Glu treatment, we observed reduction of FL amount (Fig. 5A, top) and Ncad/CTF2 production (Fig. 5A, bottom), indicating that N-cadherin was cleaved to produce Ncad/CTF2 in the mature neurons. Ncad/CTF2 production was inhibited in the presence of DFK (Fig. 5B).

Consistently, Glu treatment caused increased β-catenin level in the primary neurons, and this phenomenon was blocked by DFK (Fig. 5C, top), indicating that Ncad/CTF2 production after Glu treatment may lead to β-catenin accumulation in the neurons as well. Glu treatment reduced the level of Ser33/37/Thr41 phosphorylation (Fig. 5C, bottom, DFK(−)). After the combined treatment of Glu and DFK for 6 h, the level of phosphorylated β-catenin was higher (Fig. 5C, bottom, 50 μMDFK) when compared to Glu treatment only (Fig. 5C, bottom, DFK(−)). These results indicate that Ncad/CTF2-mediated inhibition of GSK3β was involved in the accumulation of β-catenin. The phosphorylated/total β-catenin ratio was significantly higher in the presence of DFK 6 h after Glu treatment (Fig. 5D). Finally, we examined the impact of N-cadherin cleavage on PS1/N-cadherin/β-catenin complex in neurons. In the total cell lysates, cellular N-cadherin level decreased, whereas β-catenin level increased after Glu treatment (Fig. 5E, left). In contrast, both the bindings of N-cadherin and β-catenin to PS1 decreased after Glu treatment (Fig. 5E, right), indicating that N-cadherin and β-catenin were released from PS1 after Glu treatment.

β-Catenin has been considered to be a player with two faces; supporting cytoskeletal architecture by linking cadherins to the actin cytoskeleton, and as a central player of the β-catenin nuclear signaling pathway. Although, the dual roles of β-catenin have largely been studied in isolation [30], our results provide evidence that these pathways are interconnected via ε-cleavage of N-cadherin. Membrane-bound β-catenin is released from the cadherin–catenin complex into the cytoplasm following ε-cleavage of zN-cadherin. Once released from the membrane complex, β-catenin becomes a transcriptionally active molecule. Developmentally, β-catenin nuclear signaling promotes the proliferation of neuronal stem cells, axonal remodeling, and synaptogenesis [5,31]. Moreover, β-catenin actively and flexibly modifies synaptic function [9,10]. Taken together, the activity-dependent modulation of β-catenin level might be an essential molecular mechanism for the synaptic plasticity.

Partial loss of PS1 function may cause impaired synaptic efficacy

Recently, conditional double knockout mice for PS1/2 in the adult brain were developed. Interestingly, these mice exhibit progressive synaptic dysfunction and neurodegeneration accompanied by hyperphosphorylated tau [32]. Moreover, a family with Pick-type dementia lacking amyloid deposits in the brain carried a PS1 mutation, which affects the splice signal of PS1 [33]. These findings suggest that partial loss of function in the PS1/γ-secretase complex could lead to neurodegeneration regardless of Aβ deposition. Indeed, we demonstrated in the present study that the FAD-linked mutation (P117L) results in an impaired production of Ncad/CTF2, which is in line with the previous

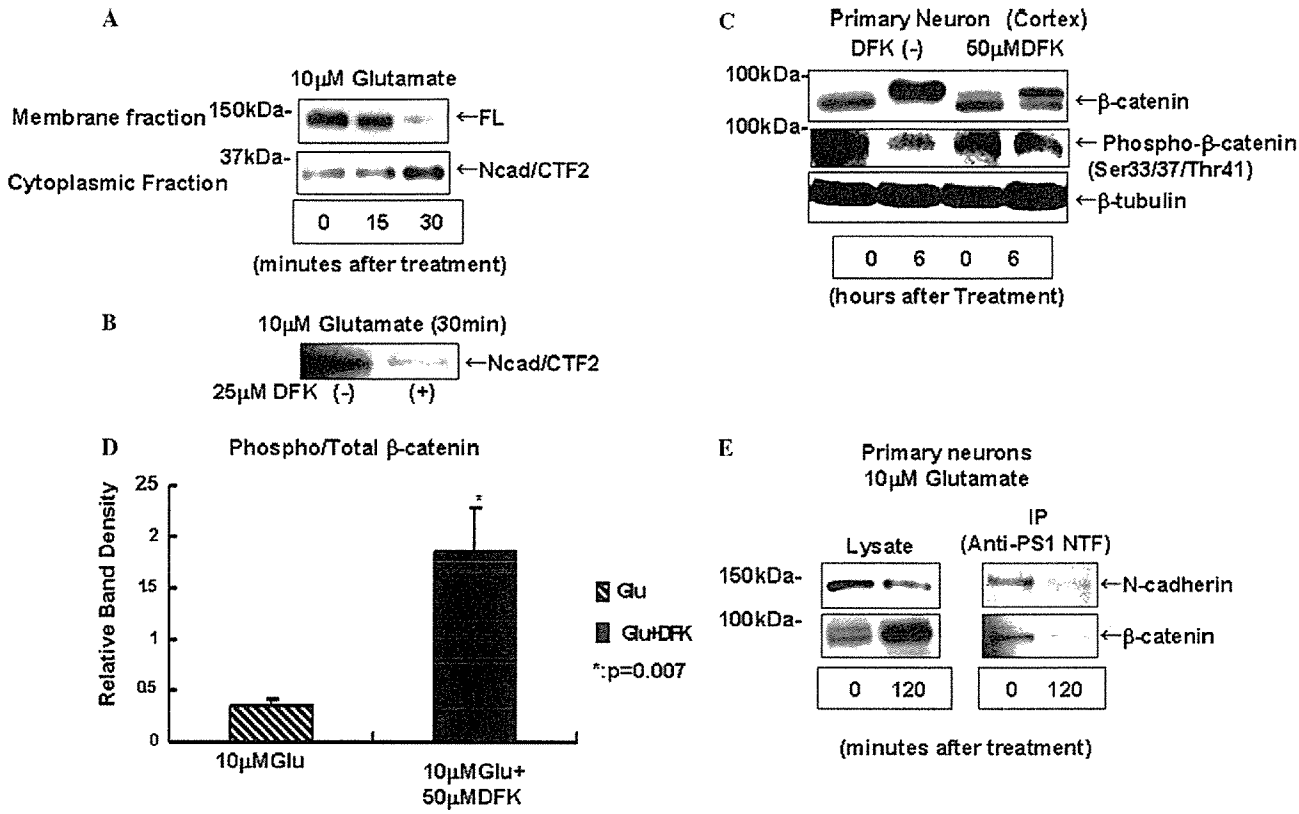

Fig. 5. β-Catenin is released from PS1/N-cadherin/β-catenin complex after Glu treatment of primary neuron. (A) Primary neurons from the rat cortex were fractionated into membrane and cytoplasmic fractions and subjected to Western blots. Ncad/CTF2 production increased with time, which is in contrast to the decrease in the levels of FL N-cadherin. (B) Primary neurons from the rat cortex were treated with 10 μM Glu in the presence or absence of 25 μM DFK. DFK inhibited the Ncad/CTF2 production. (C) β-Catenin levels were examined after Glu treatment in the absence or presence of DFK (50 μM). The accumulation of total β-catenin 6 h after Glu treatment was blocked by DFK (top). Conversely, the level of Ser33/37/Thr41 phosphorylated β-catenin was higher in the presence of DFK 6 h after Glu treatment (bottom). (D) The immunoblotting band of total and phosphorylated β-catenin 6 h after Glu treatment was quantified. The phosphorylated/total β-catenin ratio was compared between Glu treatment and Glu + DFK. The ratio was significantly higher in the presence of DFK ($n = 3$, $p = 0.007$). Data were means ± SD of three-independent experiments. (E) Primary neurons obtained from rat cortex were treated by 10 μM Glu for 120 min. Both cell lysates and immunoprecipitates by anti-PS1 antibody were subjected to Western blots. In the cell lysate, N-cadherin was decreased, whereas β-catenin was increased after Glu treatment (left). Conversely, the binding of N-cadherin and β-catenin to PS1 decreased after Glu treatment (right).

report [19]. AD begins with an impairment of memory, which is caused by a disturbance of hippocampal synaptic function [34]. Cognitive decline in AD is correlated to degree of synaptic loss [20], suggesting that partial loss of PS1 function with respect to the synaptic efficacy may be linked to AD pathogenesis. Given the accumulating evidence that β-catenin is essential for synaptic function, the dysregulation of PS1-mediated N-cadherin/β-catenin metabolism should be involved in synaptic degeneration.

Acknowledgments

We thank Drs. Y. Kaziro (Kyoto Univ) and B.T. Hyman (Harvard Medical School) for discussion and encouragement, and Dr. J. Monypenny (Kyoto Univ) for critical review, Dr. M. Kinoshita, Ms. A. Kitano, Ms. K. Odan, and Dr. H. Kimura (Kyoto University) for technical assistance, and Drs. J. Kawamata and H. Yamashita (Kyoto University) for kind advice. Financial support was provided by the Ministry of Health, Labor, and Welfare, the Ministry of Education, Culture, Sport, Science and Technology of Japan, the Smoking Research Foundation and Phillip Morris USA Inc. and Phillip Morris International.

Appendix A. Supplementary data

Supplementary data associated with this article can be found, in the online version, at doi:10.1016/j.bbrc.2006.04.157.

References

[1] A.M. Fannon, D.R. Colman, A model for central synaptic junctional complex formation based on the differential adhesive specificities of the cadherins, Neuron 17 (1996) 423–434.
[2] D.L. Benson, H. Tanaka, N-cadherin redistribution during synaptogenesis in hippocampal neurons, J. Neurosci. 18 (1998) 6892–6904.
[3] H. Togashi, K. Abe, A. Mizoguchi, K. Takaoka, O. Chisaka, M. Takeichi, Cadherin regulates dendritic spine morphogenesis, Neuron 35 (2002) 77–89.